Intercomparison of Precipitation Estimates over the Southern Ocean from Atmospheric Reanalyses

LINETTE N. BOISVERT,[a] MELINDA A. WEBSTER,[b] ALEK A. PETTY,[a,c] THORSTEN MARKUS,[a] RICHARD I. CULLATHER,[a,c] AND DAVID H. BROMWICH[d]

[a] *NASA Goddard Space Flight Center, Greenbelt, Maryland*
[b] *University of Alaska Fairbanks, Fairbanks, Alaska*
[c] *Earth System Science Interdisciplinary Center, University of Maryland, College Park, College Park, Maryland*
[d] *Byrd Polar and Climate Research Center, The Ohio State University, Columbus, Ohio*

(Manuscript received 23 January 2020, in final form 14 September 2020)

ABSTRACT: Precipitation is a major component of the hydrologic cycle and plays a significant role in the sea ice mass balance in the polar regions. Over the Southern Ocean, precipitation is particularly uncertain due to the lack of direct observations in this remote and harsh environment. Here we demonstrate that precipitation estimates from eight global reanalyses produce similar spatial patterns between 2000 and 2010, although their annual means vary by about 250 mm yr^{-1} (or 26% of the median values) and there is little similarity in their representation of interannual variability. ERA-Interim produces the smallest and CFSR produces the largest amount of precipitation overall. Rainfall and snowfall are partitioned in five reanalyses; snowfall suffers from the same issues as the total precipitation comparison, with ERA-Interim producing about 128 mm less snowfall and JRA-55 about 103 mm more rainfall compared to the other reanalyses. When compared to *CloudSat*-derived snowfall, these five reanalyses indicate similar spatial patterns, but differ in their magnitude. All reanalyses indicate precipitation on nearly every day of the year, with spurious values occurring on an average of about 60 days yr^{-1}, resulting in an accumulation of about 4.5 mm yr^{-1}. While similarities in spatial patterns among the reanalyses suggest a convergence, the large spread in magnitudes points to issues with the background models in adequately reproducing precipitation rates, and the differences in the model physics employed. Further improvements to model physics are required to achieve confidence in precipitation rate, as well as the phase and frequency of precipitation in these products.

KEYWORDS: Atmosphere; Southern Ocean; Precipitation; Rainfall; Snowfall; Reanalysis data

1. Introduction

The hydrologic cycle helps to modulate the global climate, weather patterns (Zhang 2005; Sobel et al. 2008, 2010; Tromeur and Rossow 2010), and weather extremes (Cohen et al. 2014; Overland et al. 2016) and to supply the continents with freshwater that is vital for human, animal, and biota sustainability and survival (Watkins et al. 2007). The Southern Ocean, which makes up 15% of Earth's surface (Huang et al. 2016), plays a key role in Earth's hydrologic cycle. Specifically, precipitation, a key component of the hydrologic budget (or freshwater budget) of the polar regions (Bromwich et al. 1995; Trenberth 2011; Lewis et al. 2012), contributes a significant input of freshwater to the Southern Ocean (Pauling et al. 2016). Input of freshwater via precipitation into the Southern Ocean has led to a freshening of the ocean surface in recent decades (Durack et al. 2012; de Lavergne et al. 2014). This freshening has been shown to cause stronger ocean stratification, a reduction in oceanic vertical heat transfer, and surface cooling and thus an increase in sea ice cover (Martinson 1990; Marsland and Wolff 2001; Goosse and Zunz 2014).

Precipitation that falls as snow and accumulates over sea ice is also of increasing interest to modelers, as the adequate representation of surface processes may be important for simulating conditions on local, regional, and larger scales. Snow-covered sea ice has a higher albedo than bare ice and a significantly higher albedo than open water (Warren 1982; Perovich et al. 2002). Snow is also highly insulative, so the presence and state of snow on top of sea ice inhibits the exchange of heat between the ocean and the atmosphere, and strongly modulates the sea ice growth and melt throughout the year (Sturm et al. 2002; Stammerjohn and Maksym 2017; Webster et al. 2018).

Annual precipitation tends to be greater over the Southern Ocean compared to the Arctic Ocean, and tends to be largely supplied by synoptic cyclone events accompanied by strong winds (King and Turner 1997; Turner and Pendlebury 2004; Papritz et al. 2014). This is due to the pervasive circumpolar baroclinic zone centered over the Southern Ocean and the atmospheric moisture source of the ice-free waters to the north (Tietäväinen and Vihma 2008; Sodemann and Stohl 2009). This contrasts with the mostly landlocked and synoptically isolated Arctic Ocean, where higher precipitation is mostly limited to the North Atlantic storm track (Lindsay et al. 2014; Boisvert et al. 2018).

In addition to the prognostic modeling of surface properties, snow on sea ice is important for diagnostically determining sea

Supplemental information related to this paper is available at the Journals Online website: https://doi.org/10.1175/JCLI-D-20-0044.s1.

Corresponding author: Linette Boisvert, linette.n.boisvert@nasa.gov

DOI: 10.1175/JCLI-D-20-0044.1

ice thickness and volume in both the Arctic and Southern Oceans from remotely sensed freeboard, such as NASA's *Ice Cloud and Elevation Satellite 2* (*ICESat-2*) laser altimeter (Markus et al. 2017) and the European Space Agency's (ESA) *CryoSat-2* radar altimeter (Wingham et al. 2006). Uncertainty in snow loading is thought to provide the largest source of uncertainty in these estimates (Giles et al. 2008). There are still many factors that hinder our understanding of snow depth distributions on sea ice region wide (Webster et al. 2018). The build-up and evolution of the snowpack involve complex processes including aging snow/compaction, melting/freezing, flooding, sublimation, snow loss into leads, drift/dune formation due to wind forcing, and snow lost due to sea ice convergence in the dynamic ice pack (Worby et al. 1998; Massom et al. 2001; Kwok et al. 2017; Webster et al. 2018). Nevertheless, the amount and type of precipitation are the fundamental variables for determining the snow mass on sea ice. Particularly in the Antarctic environment, our understanding of snow mass is critically limited due to the scarcity of basin-scale observations (Massom et al. 2001; Sturm and Massom 2017). Thus, there is a heavy reliance on simulating snow thickness accurately via modeling efforts, which requires 1) good representation of snow processes and 2) accurate precipitation forcing.

The accurate simulation of precipitation faces considerable challenges, however, with the greatest being our limited knowledge of clouds, convection, boundary layer processes, and other cloud microphysical properties at high latitudes (e.g., Lubin et al. 1998; Dai 2006; Bromwich et al. 2012; Boisvert et al. 2018). It was recently shown by Boisvert et al. (2018) that over the Arctic Ocean, precipitation across eight reanalyses varies significantly in terms of amount, phase and frequency. Bromwich et al. (2011) and Nicolas and Bromwich (2011) completed an assessment of precipitation across six reanalyses between 1979 and 2009 for both Antarctica and the Southern Ocean and found varying trends across products. Bromwich et al. (2011) and Nicolas and Bromwich (2011) attributed the differences in trends to changes in observing systems and availability of satellite data ingested into the assimilation systems. In the Southern Ocean, unlike the Arctic, in situ observations may often be thousands of kilometers away from a given location. While numerical weather prediction skill has become comparable to that of the Northern Hemisphere (Bauer et al. 2015), the dependence on remote sensing data in the Southern Hemisphere means that changes in the satellite observing systems could have a larger impact on temporal spatial trends compared to the Arctic Ocean.

Verification of modeled precipitation is also fraught with difficulties dealing with the lack of measurements both spatially and temporally in the polar regions, such as those arising from gauge undercatchment biases, blowing snow, difficulties in measuring trace precipitation (e.g., diamond dust), rime ice formation, and the feasibility of collecting measurements in such a vast and extreme environment (Sevruk 1982; Yang et al. 1995; Goodison et al. 1998; Adam and Lettenmaier 2003; Serreze et al. 2005). Remote sensing of precipitation has provided new opportunities to assess modeled precipitation, but it also has its own set of difficulties, where the strengths and weaknesses in measuring different aspects of precipitation are unique to each satellite sensor (Haynes et al. 2009; Behrangi et al. 2012, 2014). Here, as with modeling snow, satellite products are difficult to validate and suffer from a lack of observations. This is particularly true over the Southern Ocean where in situ observations of precipitation rate are rare, hindering validation efforts.

In this study, we update previous intercomparisons by using output from eight reanalyses, including ERA5 [the fifth major global reanalysis produced by the European Centre for Medium-Range Weather Forecasts (ECMWF)], and compare the precipitation amount, frequency, and phase across the Southern Ocean. We focus on the contemporary period (2000–16) to avoid large jumps in the reanalyses data that might be caused by large changes in the number of assimilated datasets as found by Bromwich et al. (2011). Leveraging remotely sensed observations, snowfall derived from *CloudSat* retrievals over the whole Southern Ocean are also utilized to evaluate reanalyses snowfall amount. The full domain of the Southern Ocean does not fall within the *CloudSat* ''pole hole,'' allowing for optimal coverage and assessments. Data from snow buoys in the Weddell Sea (Nicolaus et al. 2017; Grosfeld et al. 2016) were also explored to determine whether their quality was sufficient for evaluating reanalysis precipitation in the Southern Ocean.

2. Data

a. *Reanalyses*

The eight reanalyses used in this study are the following:

1) NASA's Modern-Era Retrospective Analysis for Research and Application (MERRA; Rienecker et al. 2011);
2) MERRA version 2 (MERRA-2; Gelaro et al. 2017);
3) European Center for Medium-Range Weather Forecasts (ECMWF) interim analysis (ERA-Interim; Dee et al. 2011);
4) ECMWF Reanalysis version 5 (ERA5; Hersbach et al. 2020);
5) National Centers for Environmental (NCEP)–Department of Energy (DOE) reanalysis (NCEP R2; Kanamitsu et al. 2002);
6) NCEP Climate Forecast System Reanalysis (CFSR; Saha et al. 2010);
7) Japanese 55-year Reanalysis (JRA-55; Kobayashi et al. 2015); and
8) National Oceanographic and Atmospheric Administration (NOAA)–University of Colorado Cooperative Institute for Research and Environmental Sciences (CIRES) Climate Diagnostics Center, Twentieth Century Global Reanalysis version 2 (NOAA-CIRES; Compo et al. 2009).

The reanalyses are described in more detail in the supplemental section and are summarized in Table 1. The NCEP–National Center for Atmospheric Research (NCAR) reanalysis (NCEP R1; Kalnay et al. 1996) is not included in this study, as there is a physical ringing pattern in the precipitation variables at high latitudes, which was removed in NCEP R2 (e.g., Lindsay et al. 2014; Boisvert et al. 2018). An example

TABLE 1. Descriptions of the nine reanalyses used in this study (IAU is incremental analysis update).

Reanalysis	Fields used	Grid spacing	Assimilation method	Sea ice cover	Microphysics scheme
JRA-55	2000–16; daily precipitation, snowfall	63 km	4D-Var	Daily (Ishii et al. 2005); threshold cover	Prognostic cloud condensate (Sundqvist 1998); condensate PDF (Smith 1990)
ERA-Interim	2000–16; daily precipitation, snowfall	78 km	4D-Var	Weekly and daily, multiple sources; fractional	Prognostic cloud condensate (Tiedtke 1993); condensate PDF (Tompkins 2002)
ERA5	2000–16; daily precipitation, snowfall	31 km	Ensemble 4D-Var	Daily Satellite Application Facility on Ocean and Sea Ice (OSI-SAF) product; fractional	Prognostic cloud condensate (Tiedtke 1993) updated from 3–6 moisture related prognostic variables; condensate PDF (Tompkins 2002; Sotiropoulou et al. 2015)
MERRA	2000–15; daily precipitation, snowfall	74 km	3D-Var/IAU	Weekly (Reynolds et al. 2002); fractional	Prognostic cloud condensate (Bacmeister et al. 2006)
MERRA-2	2000–16; daily precipitation, snowfall	69 km	3D-Var/IAU	Daily (Reynolds et al. 2007), OSTIA; fractional	Prognostic cloud condensate (Bacmeister et al. 2006); condensate PDF (Molod 2012)
NCEP R1	2000–16; daily precipitation	208 km	3D-Var	Daily (Grumbine 1996); threshold cover	Layer saturation
NCEP R2	2000–16; daily precipitation	208 km	3D-Var	Daily (Grumbine 1996); threshold cover	Layer saturation
CFSR	2000–10; daily precipitation	38 km	3D-Var	Daily NASA (Grumbine 1996); fractional	Prognostic cloud condensate (Moorthi et al. 2001)
NOAA-CIRES V2c	2000–14; daily precipitation	200 km (2° × 2°)	Ensemble Kalman filter (Compo et al. 2011)	Monthly COBE-SST2 sea ice (Hirahara et al. 2014)	Prognostic cloud condensate (Moorthi et al. 2001)

of this pattern is shown in Fig. S1 in the online supplemental material.

Daily total precipitation data from all reanalyses are used in this study, along with daily snowfall rates, which are only available from ERA-Interim, ERA5, MERRA, MERRA-2, and JRA-55. Since not all of the reanalyses cover 2000–16, only the 2000–10 time period is used in the annual means and comparisons. All of the daily precipitation products are converted to water-equivalent millimeters per day and are regridded to the standard 25 km^2 polar stereographic grid (Maslanik and Stroeve 1990) using a bilinear interpolation method.

In this study we focus on the oceanic regions outlined in Fig. 1. When we refer to the Southern Ocean we are referring to all of the oceanic regions in Fig. 1, which is different from a standard hydrographic definition of ocean below 60°S. It is important to note here that the Southern Ocean study area (Fig. 1) is not completely square and extends to different latitudes in each region. Some of the regions have more open ocean (e.g., Pacific Ocean) and others have more sea ice cover (e.g., Weddell Sea). Some regions' ocean areas begin at lower latitudes due to the location of the Antarctic continent compared to others. The reanalyses' precipitation products might be affected based on the amount of sea ice coverage in the area because while in situ observations are assimilated over Antarctic sea ice, there are few to no observations, and passive microwave observations are often not assimilated over areas with sea ice coverage (Dee et al. 2011), so regions with larger sea ice coverage might be more variable between products.

b. *CloudSat*

NASA's *CloudSat* satellite was launched in April 2006 (Stephens et al. 2008) and remains operational; in 2011, *CloudSat* switched to a daytime only mode due to a battery power failure, requiring sunlight for it to operate. The Cloud Profiling Radar (CPR) onboard is used to produce cloud and precipitation products. The CPR produces reflectivity profiles in the lowest 30 km of the atmosphere (Tanelli et al. 2008). Precipitation is estimated from these profiles, together with cloud microphysical assumptions and temperatures from ECMWF Operational Analyses (Kulie and Bennartz 2009; Wood et al. 2013). The monthly gridded 2C-SNOW-PROFILE (2C-SNOW) *CloudSat* product used here is near-surface snow and is produced from the orbital data profiles on a 1° × 1° grid, where Southern Ocean overpasses occur on average every 3 to 10 days (Milani et al. 2018). *CloudSat* snowfall products have previously been used in other studies over the Antarctic and Southern Ocean (Palerme et al. 2014; Milani et al. 2018; Souverijns et al. 2018), although validation in these

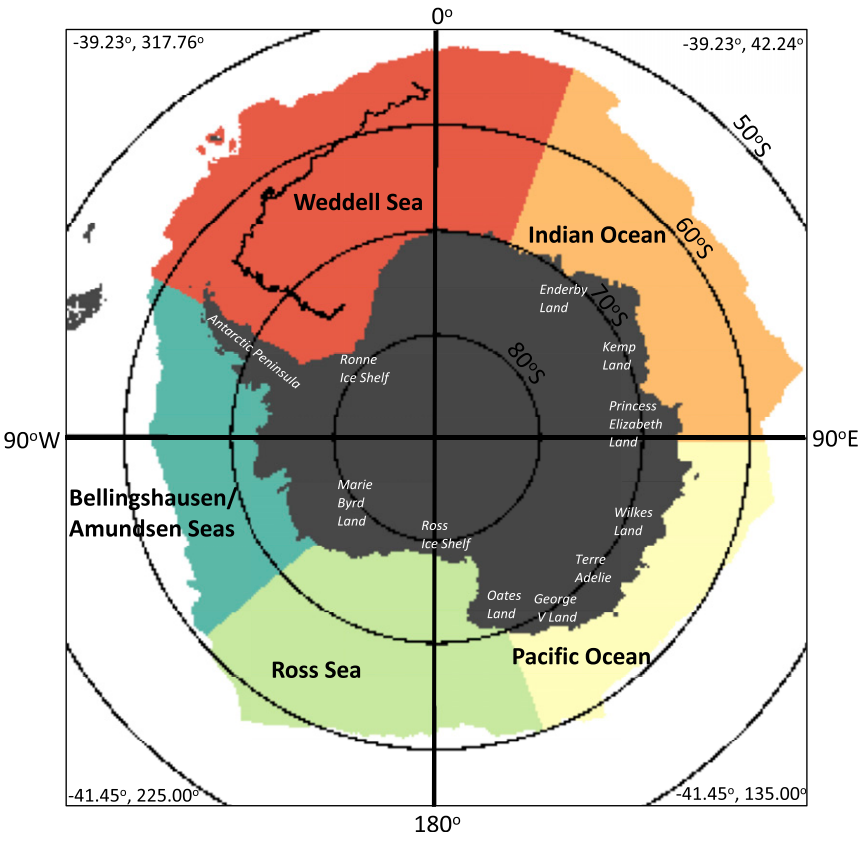

FIG. 1. Ocean region mask of the Southern Ocean surrounding the Antarctic continent. Maximum sea ice extent between 2000 and 2016 is shown for each region in color. Each region comprises the maximum sea ice extent (color) and ice-free ocean (white) areas. Land is dark gray, and locations referenced in the text are in white. The Southern Ocean comprises all regions in this figure north of the Antarctic continent. The region mask is taken from https://nsidc.org/. The 2014S9 buoy track (black squiggly line) is displayed in the Weddell Sea and is in reference to Fig. 14.

data-sparse areas is difficult (Kulie and Bennartz 2009; Behrangi and Richardson 2018).

c. *Snow buoys*

Nine snow buoys (Nicolaus et al. 2017; Grosfeld et al. 2016) deployed by the Alfred Wegener Institute (AWI) in the Weddell Sea in 2013–16 were used to assess reanalysis precipitation events and reanalysis-derived snow depths (excluding CSFR, which is only available until 2010). Each buoy is equipped with four sonic-ranging sensors, from which hourly snow depth can be determined, and an air temperature sensor. For this study, we took the median of the four snow depth retrievals and averaged them over 24 h for comparisons with the reanalysis products. The median was chosen for two reasons: First, given the small sample size (~3–4 sonic range finder points per buoy) and large noise in the buoy data (see point below), the median provides a more stable value than the mean and second, even though the snow buoys provide ~3–4 point measurements, the noise in the data is large enough to have an erroneous effect on the average, which is more sensitive to outliers than taking the median of small sample sizes. In the buoy data, a "snowfall event" was defined as any day that the snow depth increased by 1 cm or more, which is the accuracy of the sonic-ranging sensors. Precipitation amounts less than 1 mm day^{-1} from reanalysis products were excluded from the comparisons due to the erroneously high frequency of small precipitation in reanalysis products (Boisvert et al. 2018) and because the sonic-range sensors only have an accuracy of 1 cm. An example that includes all precipitation is shown in Fig. S2 for reference.

3. Results: Comparisons of precipitation estimates across reanalyses

a. *Magnitude of precipitation*

Figure 2 shows the 2000–10 mean annual total precipitation and spread from each of the eight reanalyses. Spatially, all

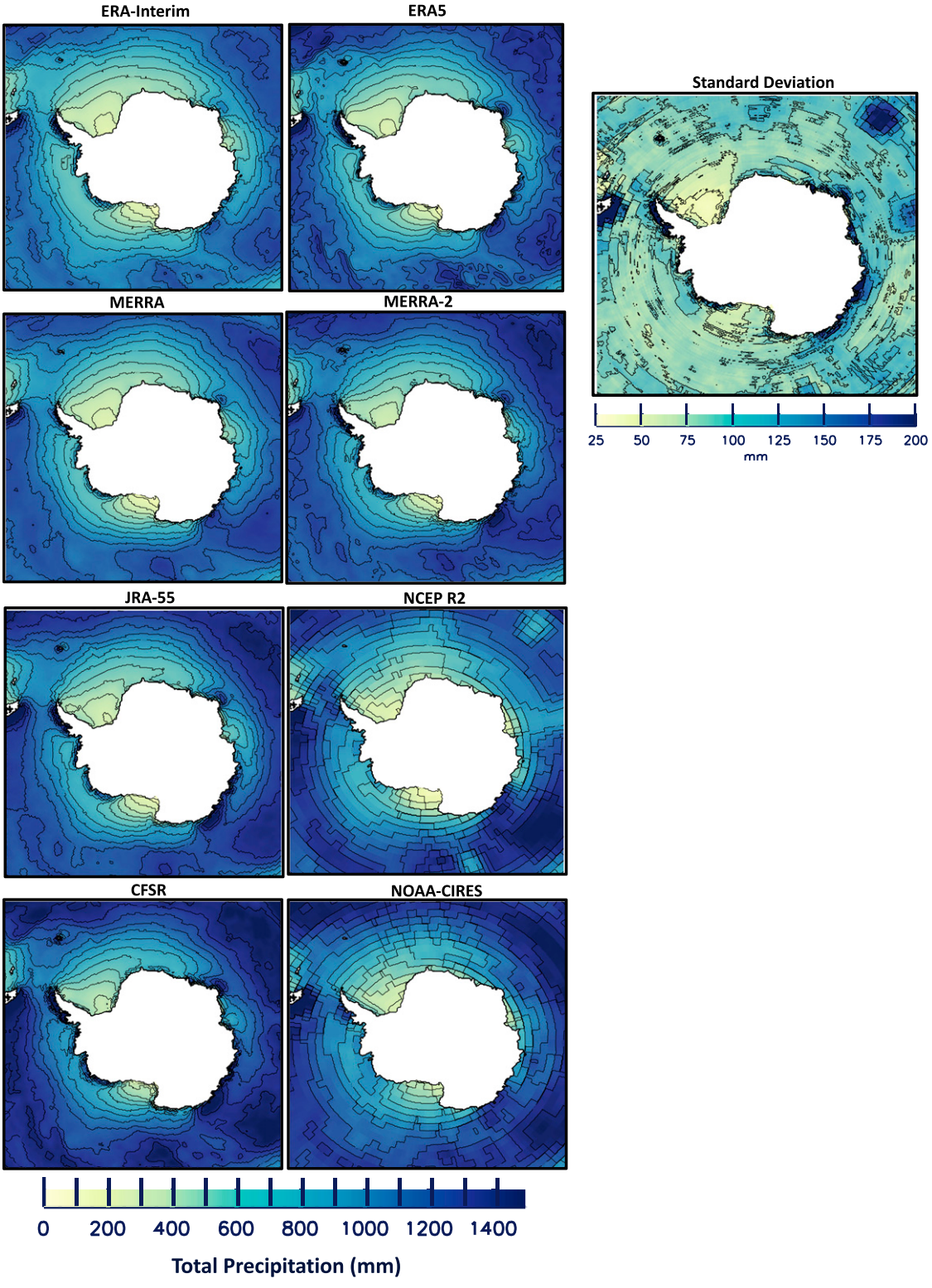

FIG. 2. Average 2000–10 annual total precipitation (mm) in the Southern Ocean for each of the reanalyses. The standard deviation (mm) is shown on the right. Contour lines in the figures represent the contour lines on the color bars.

TABLE 2. Average 2000–10 annual cumulative precipitation and interannual standard deviations (in parentheses) for each reanalysis. The regions are outlined in Fig. 1. All values in the table are in millimeters.

	Southern Ocean	Weddell Sea	Indian Ocean	Pacific Ocean	Ross Sea	Bellinghausen/Amundsen Seas
ERA-Interim	826.9 (14.7)	739.7 (14.4)	856.1 (19.8)	914.6 (24.5)	815.2 (22.4)	925.8 (50.4)
ERA5	921.6 (16.5)	828.2 (19.6)	960.3 (20.0)	1015.7 (26.1)	910.5 (26.3)	1020.0 (54.5)
MERRA	890.6 (32.9)	789.7 (38.5)	900.8 (49.5)	998.7 (35.9)	907.5 (34.0)	994.6 (50.7)
MERRA-2	979.7 (16.6)	895.1 (16.9)	1033.2 (29.7)	1081.6 (25.3)	957.5 (22.9)	1058.1 (45.1)
JRA-55	935.1 (14.8)	877.9 (20.3)	1015.4 (18.7)	997.7 (21.8)	819.9 (20.5)	1076.5 (51.4)
NCEP R2	934.1 (22.2)	821.6 (44.0)	867.2 (40.7)	1101.3 (25.6)	962.1 (31.2)	1075.1 (53.0)
CFSR	1071.8 (26.7)	961.0 (23.8)	1109.2 (25.3)	1175.5 (34.6)	1070.4 (28.4)	1183.6 (65.8)
NOAA-CIRES	1013.1 (11.1)	930.3 (16.2)	1047.2 (21.1)	1119.7 (20.6)	986.2 (26.0)	1116.1 (40.1)

reanalyses show precipitation generally increasing northward (lower latitudes) from the Antarctic continent. This latitudinal gradient could be caused by the extent and variability of sea ice coverage and how this affects the cyclone storm tracks and the moisture source. The only area where this does not occur is off of the coast of Terre Adelie and Wilkes Land in the South Pacific Ocean sector (Fig. 1), where no clear latitudinal gradient occurs. This could be because the sea ice edge is much closer to the continent in these areas, whereas in the other areas the sea ice coverage is much larger and extends to lower latitudes, especially during the winter months. All reanalyses produce the least amount of precipitation in the Weddell and Ross Seas. While the reanalyses show similar spatial patterns, their magnitudes show clear differences of about 250 mm yr^{-1} across products. While ERA-Interim has the least precipitation averaged over 2000–16 across the entire Southern Ocean (827 mm yr^{-1}), CFSR (1072 mm yr^{-1}) and CIRES (1013 mm yr^{-1}) have the highest amounts (Table 2). This is similar to the ranking in the magnitude of reanalyses precipitation in the intercomparison in the Arctic Ocean (e.g., Boisvert et al. 2018).

The largest spread between the reanalyses (Fig. 2) occurs in regions where annual precipitation rates are the largest and where there is reduced sea ice cover–in the Indian Ocean sector at lower latitudes (top right of the figure). Large differences also occur close to the Antarctic continent in the Indian and Pacific sectors, and to the west of the Antarctic Peninsula in the Bellingshausen/Amundsen Seas. NCEP/CIRES produces more precipitation adjacent to the Antarctic coastline in the Indian and Pacific Ocean regions, while JRA-55 produces smaller amounts in these same areas. As compared to the reanalyses average, NCEP-R2 has smaller regions of much lower precipitation in the southern (higher latitudes) regions of the Weddell Sea and Indian Ocean.

Figure 3 shows the time series of regional mean annual total precipitation for the sectors in Fig. 1. The figure indicates spread and magnitude differences that are similar to those for the Arctic Ocean (e.g., Boisvert et al. 2018). But unlike the Arctic Ocean, MERRA-2 and NCEP-R2 are not consistent in their representation of interannual precipitation variability compared to the other reanalyses. These consistencies exist in some regions; for example, many time series share similar features in the Pacific Ocean and the Ross and Bellingshausen/Amundsen Seas. Similar to the Arctic Ocean, CFSR has the highest magnitude in precipitation, but the lowest values are from ERA-Interim in 2000–10, and for MERRA for 2010–15. MERRA has a large decrease in precipitation in 2000–15 and ERA-Interim has a slight increase. JRA-55, ERA5, and NCEP-R2 all have similar magnitudes in precipitation for the Southern Ocean (Fig. 3a). MERRA-2 has interannual variability similar to ERA5 and JRA-55, although the magnitude is about 50 mm yr^{-1} larger for MERRA-2 (Table 2). The ranking of the reanalyses by precipitation amount changes for the different regions; however, CFSR always remains the largest. A close evaluation of time series and their potential relation to changes in the observing system is beyond the scope of this paper. Nevertheless, some issues are apparent. The introduction of the Advanced Microwave Sounding Unit (AMSU) in November 1998 is well known to have affected reanalysis time series, and is thought to have had a particularly adverse impact on MERRA over the Southern Ocean (Bosilovich et al. 2011; Cullather and Bosilovich 2011; Nicolas and Bromwich 2011). Cullather and Bosilovich (2011) found that MERRA Southern Ocean precipitation increased by 40% with the introduction of AMSU. For high latitudes, reanalyses have a particular dependence on passive microwave observations. The loss of radiance data from Defense Meteorological Satellite Program (DMSP) satellites *F14* in August 2008 and *F13* in November 2009, and the inability of older reanalyses to incorporate newer sensors (Gelaro et al. 2017) likely plays some role in the differences seen after 2008. Over that time period, MERRA precipitation decreases by more than 10%, in contrast with other reanalyses. It is important to note that NOAA/CIRES is not affected by changes in satellite observations because it only assimilates sea level pressure.

In the Ross Sea (Fig. 3e), JRA-55 (purple line) has the lowest precipitation (820 mm yr^{-1}), very similar to the magnitude of ERA-Interim, whereas in all other regions JRA-55 falls in the middle of the distribution. The products show similar interannual variability in the Weddell, Bellingshausen/Amundsen, and Ross Seas, except for MERRA and ERA-Interim in the Weddell Sea and MERRA in the Ross Sea, where clear increases or decreases in precipitation occur over the time period (Fig. 3). In the Pacific and Indian Ocean regions, all reanalysis products tend to be more inconsistent in the magnitude and interannual variability (Figs. 3c,d). In the Pacific and Indian Oceans and in the Ross and Bellingshausen/Amundsen Seas, ERA-Interim and ERA5 show similar interannual variability, but the magnitude of ERA5 is

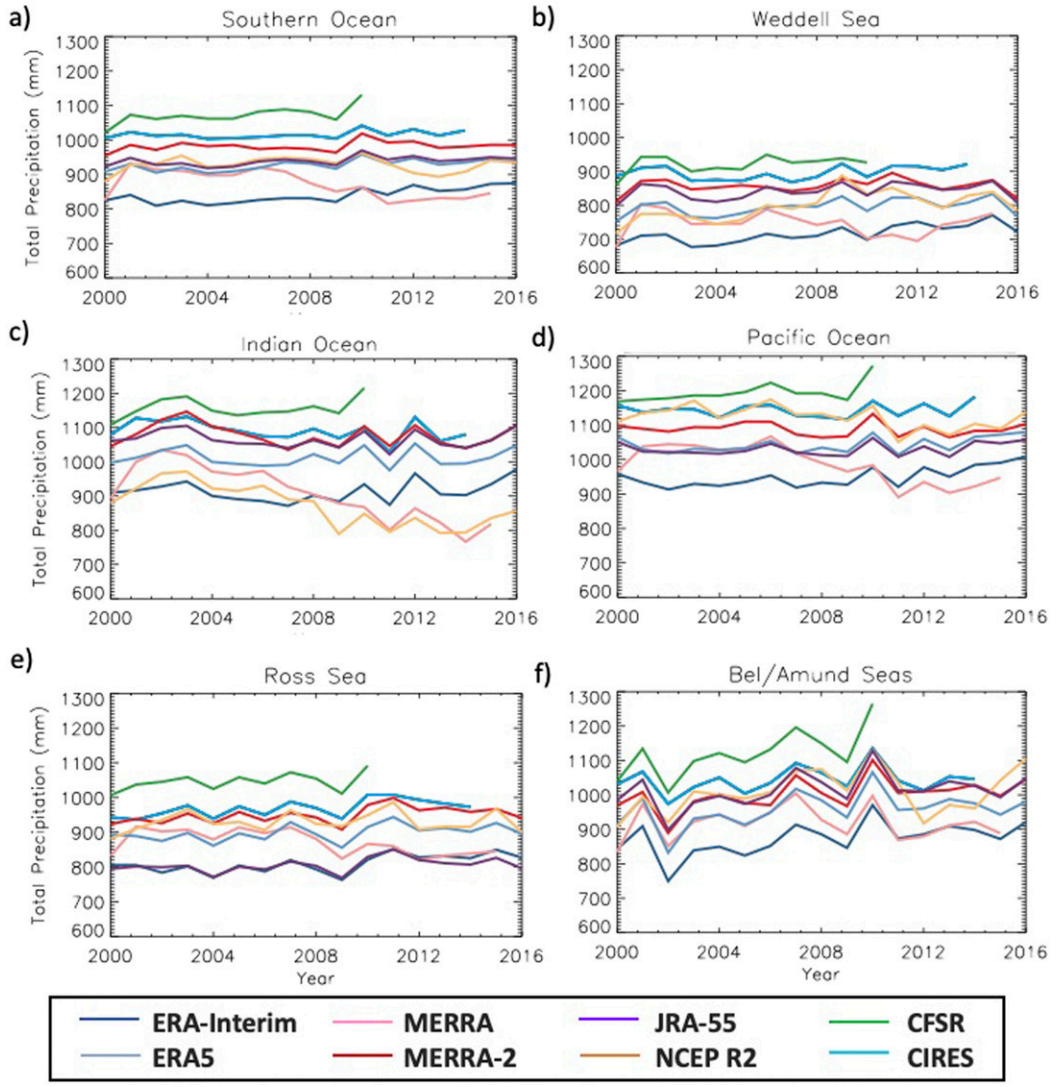

FIG. 3. Cumulative yearly precipitation from each reanalysis from 2000 to 2016 averaged over each of the regions: (a) the Southern Ocean (entire domain in Fig. 1), (b) Weddell Sea, (c) Indian Ocean, (d) Pacific Ocean, (e) Ross Sea, and (f) Bellingshausen/Amundsen Seas. Note that the *y* axis does not start at zero.

consistently about 100 mm yr^{-1} higher than ERA-Interim (Fig. 3 and Table 2).

The magnitudes of the monthly total precipitation from 2000 to 2010 for the Southern Ocean and regions therein (Fig. 1) are shown in Fig. 4. Similar to the annual precipitation, the spread in the magnitude of monthly precipitation across the products is large, with a maximum difference of about 20 mm $month^{-1}$. CFSR has the largest monthly precipitation across the Southern Ocean, with MERRA and ERA-Interim producing the lowest (Fig. 4a). The monthly precipitation across the Southern Ocean reaches its peak in March (during the austral fall), decreasing in the austral winter and spring and reaching its minimum between November and January (summer). Although NOAA-CIRES has similar monthly precipitation as JRA-55 from January–March, NOAA-CIRES remains larger for the remainder of the year (Fig. 4a). ERA5, JRA-55, MERRA-2, and NCEP R2 all have similar magnitudes of monthly precipitation. The annual cycle is consistent with other findings that show the highest precipitation in the Southern Ocean occurs in the fall and winter months due to increased cyclone activity (Bromwich 1988).

The regional analysis highlights the differing monthly cycles in precipitation. For example, the Weddell Sea has the highest precipitation in March, with its minimum in November across all products, similar to the Southern Ocean (Fig. 4b). The Indian Ocean has its peak in precipitation in May, and the Pacific Ocean has its peak in March, with the Pacific Ocean having slightly more precipitation between March–September compared to the Indian Ocean. Both regions have a decrease in precipitation between October–December, with the Pacific (Indian) Ocean region reaching its minimum in November

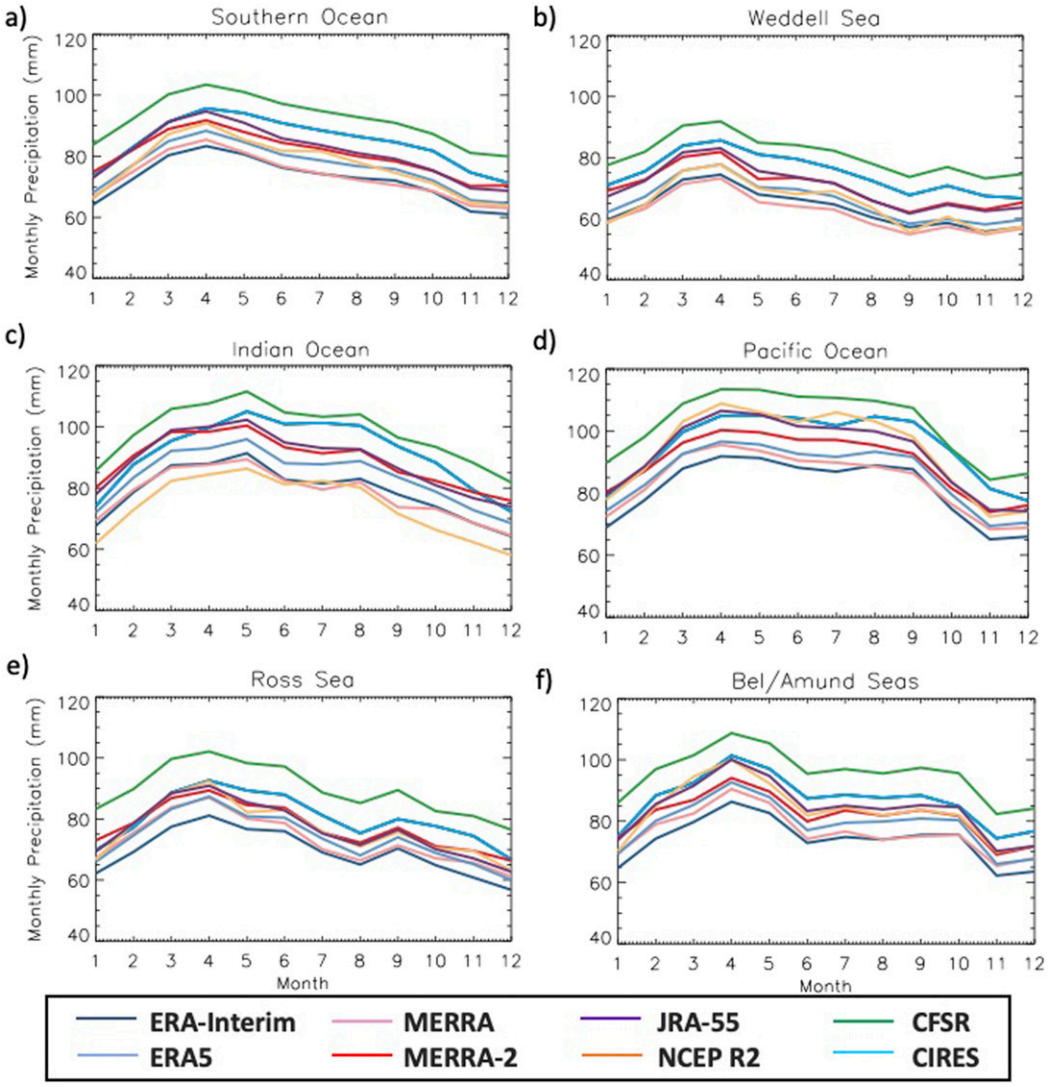

FIG. 4. Average 2000–10 cumulative monthly precipitation for (a) the Southern Ocean (entire domain in Fig. 1), (b) Weddell Sea, (c) Indian Ocean, (d) Pacific Ocean, (e) Ross Sea, and (f) Bellingshausen/Amundsen Seas. Note that the *y* axis does not start at zero.

(December) (Figs. 4c,d). The Ross Sea has a secondary peak in precipitation in September, although this is approximately ~15 mm month^{-1} smaller than April (Fig. 4e). This secondary peak is consistent across the products. The Bellingshausen/Amundsen Seas show a peak in April and then a decrease in precipitation to a nearly constant amount in June–October before finally decreasing again (Fig. 4f).

b. Magnitude of snowfall and rainfall

Only five of the eight reanalyses in this study provide a snowfall product: ERA-Interim, ERA5, JRA-55, MERRA, and MERRA-2. The average annual cumulative snowfall in 2000–10 for each reanalysis along with their spread (standard deviation) across the products are shown in Fig. 5. Similar to total precipitation, the least amount of snowfall occurs in the Weddell and Ross Seas, closest to the Antarctic continent, and increases toward lower (more northerly) latitudes (Fig. 5). Unlike total precipitation, snowfall decreases in magnitude northward (lower latitudes) from the continent until about 65°S, where it drops off rapidly to zero as it encounters warmer atmospheric temperatures at the lower latitudes. All of the five reanalyses agree with this transition and have some of the smallest standard deviations just north of this zone.

The largest amount of snowfall occurs just off the East Antarctic coast, from Terre Adelie to Princess Elizabeth Land, and slightly farther west between Kemp Land and Enderby Land (Fig. 5). These same spatial patterns are seen across the five reanalyses, but the magnitude of the snowfall varies. For instance, the average annual snowfall in the Southern Ocean ranges between 250 and 450 mm yr^{-1}, with ERA-Interim

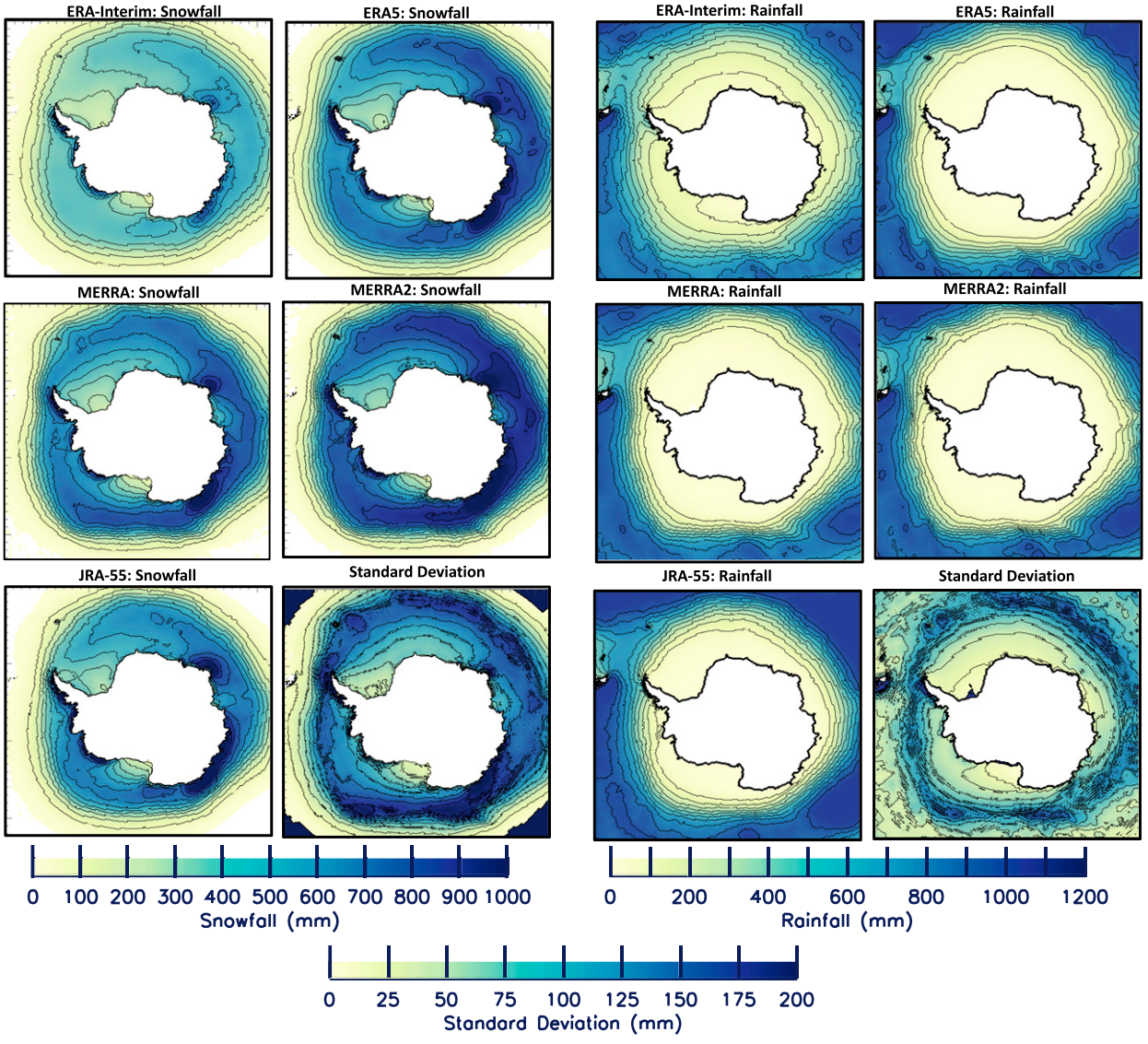

FIG. 5. Average 2000–10 annual cumulative (left) snowfall and (right) rainfall (mm yr^{-1}). The standard deviation (mm) is shown on the bottom right for both snowfall and rainfall. Contour lines in the figures represent the contour lines on the color bars.

producing the least and MERRA-2 producing the most (Table 3). The least variable snowfall occurs in the Weddell and Ross Seas closest to the continent. The most variable snowfall between the products occurs between 55° and 65°S, where most of the precipitation occurs and is likely a result of the variability in the snow to rain transition location across products (Fig. 5).

The annual-average snowfall between 2000 and 2016 from each reanalyses for the full Southern Ocean domain and for individual regions is shown in Fig. 6. There is a large spread

TABLE 3. Average 2000–10 annual snowfall and interannual standard deviations (in parentheses) for each reanalysis. The regions are outlined in Fig. 1. All values in the table are in millimeters.

	Southern Ocean	Weddell Sea	Indian Ocean	Pacific Ocean	Ross Sea	Bellingshausen/Amundsen Seas
ERA-Interim	263.0 (7.5)	228.2 (9.2)	377.0 (10.1)	286.7 (19.8)	218.5 (11.3)	198.3 (22.1)
ERA5	414.8 (11.4)	364.3 (14.0)	577.4 (12.2)	459.4 (24.4)	350.3 (17.9)	324.4 (33.0)
MERRA	387.7 (12.7)	354.7 (24.7)	525.6 (26.0)	441.2 (21.7)	337.5 (12.9)	278.4 (13.5)
MERRA-2	453.8 (7.4)	421.2 (12.7)	628.6 (19.0)	503.0 (26.4)	384.0 (13.6)	324.4 (23.4)
JRA-55	307.7 (4.6)	273.4 (12.0)	442.2 (8.0)	347.5 (16.0)	265.7 (6.5)	181.6 (15.6)

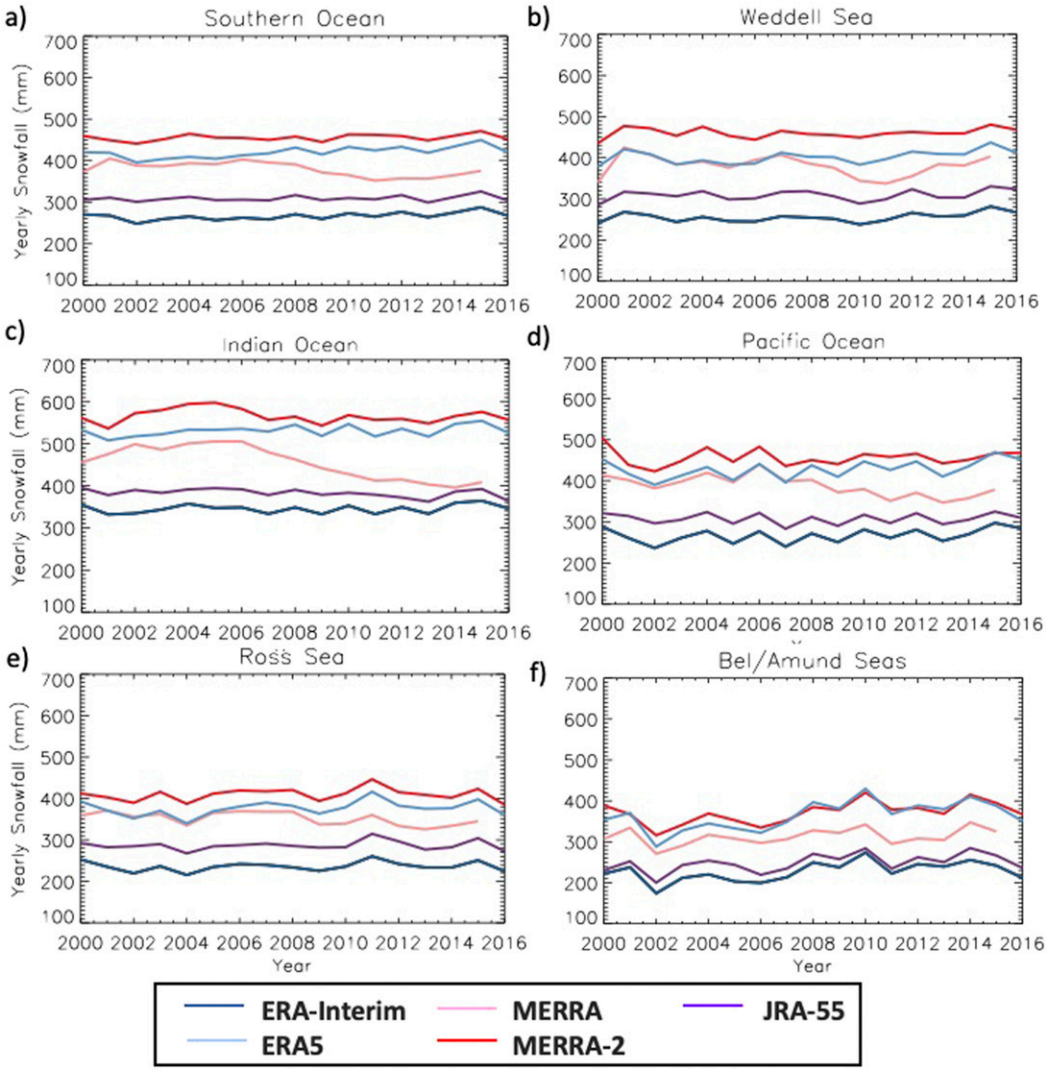

FIG. 6. Annual cumulative snowfall from 2000–16 for (a) the Southern Ocean (entire domain in Fig. 1), (b) Weddell Sea, (c) Indian Ocean, (d) Pacific Ocean, (e) Ross Sea, and (f) Bellingshausen/Amundsen Seas. Note that the *y* axis does not start at zero.

(~200 mm yr^{-1}) in the magnitude of snowfall amount the reanalyses for all regions (Fig. 6). But unlike the total precipitation comparison, there is agreement in the interannual variability between products in all of the study regions (Fig. 6). ERA-Interim produces the least amount of snowfall in all regions except for the Bellingshausen/Amundsen Seas, where both JRA-55 and ERA-Interim are the lowest (Fig. 6). MERRA-2 produces the most snowfall in all of the regions, except for the Bellingshausen/Amundsen Seas beginning in 2006, when ERA5 starts to produce more snowfall. ERA5 and MERRA-2 have similar magnitudes, with their differences being much less than the overall product spread, in snowfall in the Southern Ocean in all regions except for the Weddell Sea. ERA5 and MERRA have similar magnitudes in a few of the regions (Weddell and Ross Seas, and the Pacific Ocean) in 2000–08 and then diverge in 2008–16 (Figs. 6b,d,e). This could be attributed to the amount and type of data assimilated into each reanalysis system (Bromwich et al. 2011; Nicolas and Bromwich 2011). However, this is beyond the scope of the current study. Similar to the total precipitation analysis, MERRA shows a decrease in snowfall beginning in 2010 (Fig. 6a). MERRA also has a similar decrease in the Indian and Pacific Oceans and the Ross Sea, but not in any other regions.

The 2007–10 *CloudSat* average monthly snowfall is compared with the five reanalyses' snowfall and the results are shown in Fig. 7. Although *CloudSat* has a lower temporal sampling, it has been shown to produce fairly accurate snowfall rates when compared with ground-based radar in Antarctica (Souverijns et al. 2018; Lemonnier et al. 2019) and other datasets over Antarctica (Milani et al. 2018; Palerme et al. 2017) and is useful for regional-scale comparisons. The *CloudSat* snowfall suffers from sampling biases and ground clutter issues

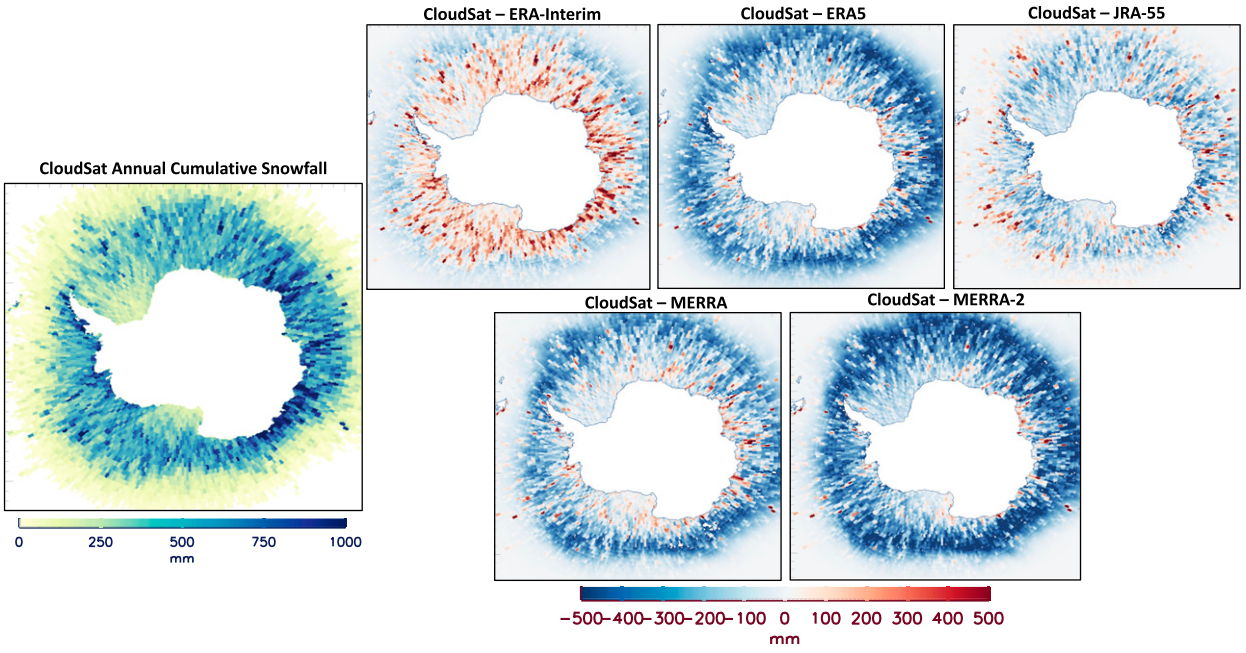

FIG. 7. Comparisons of monthly averaged *CloudSat* 2007–10 snowfall with five reanalyses' snowfall averaged monthly between 2007–10. (top left) The average 2007–10 snowfall from *CloudSat*. Other panels shown are average 2007–10 snowfall differences between *CloudSat* and ERA-Interim, ERA5, MERRA, MERRA-2, and JRA-55.

and also utilizes ECMWF Operational Analysis temperatures to partition between snowfall and rainfall. The *CloudSat* results used here should thus be treated with caution and not as ground truth.

CloudSat shows the least amount of snowfall in the Weddell and Ross Seas near the ice shelves. Higher amounts of precipitation occur in the Bellingshausen/Amundsen Seas near the Antarctic coast and Antarctic Peninsula and also in the Indian and Pacific Ocean sectors. When taking the difference in magnitude between *CloudSat* and each reanalysis, it is clear that *CloudSat* detects more snowfall than ERA-Interim (~25 mm month^{-1} less than *CloudSat*), and *CloudSat* detects much less snowfall than MERRA-2 (~35 mm month^{-1} more than *CloudSat*), specifically in the areas over the sea ice pack, closest to the continent. All of the reanalyses except ERA-Interim produce similar patterns of snowfall differences when compared to *CloudSat*, with *CloudSat* detecting much less snowfall at higher latitudes and more snowfall at lower latitudes (~60°S). The largest differences are seen in MERRA-2 and JRA-55, with ERA5 and MERRA having more similar spatial patterns. It is speculated that the temperatures and temperature threshold differences between the individual reanalyses are likely causing the latitudinal differences of the snowfall amounts between *CloudSat* and the reanalysis products, whereas for ERA-Interim, which always produces lower snowfall amounts compared to both *CloudSat* and the other reanalysis, this pattern does not appear. Although the magnitudes of snowfall are not always the same for *CloudSat* and each reanalysis, it is promising that both the remotely sensed snowfall and reanalysis snowfall show similar patterns of intensity in the Southern Ocean. Another similar pattern between *CloudSat* and all of the reanalyses precipitation is the higher precipitation on the west of the Antarctic Peninsula and the much drier conditions on the east of the peninsula.

Rainfall can also be assessed from the five reanalyses that produce snowfall as the residual of total precipitation and snowfall, with the mean (2000–10) annual rainfall shown in Fig. 5. All reanalyses agree that the least amount of rainfall occurs closest to the Antarctic continent and this increases toward lower (more northern) latitudes. However, the area with the least amount of rainfall (yellow area) varies between them. Thus, the largest deviations between the reanalyses occur in the ~60°S latitudinal band where the strong rainfall (and snowfall) transition occurs (Fig. 5). Total annual rainfall in the Southern Ocean varies around 100 mm yr^{-1} in magnitude across the five reanalyses, with JRA-55 producing the highest rainfall, followed by ERA-Interim (Fig. 8, Table 4). These two reanalyses also have the lowest snowfall amounts in the Southern Ocean, suggesting this is principally driven by the snowfall/rainfall partitioning. ERA5 has the lowest rainfall in 2001–08, while MERRA has the lowest rainfall for the remainder of the period, as its rainfall decreases over the period 2007–15 (Fig. 8a). ERA5 and MERRA-2 have very similar rainfall amounts in the Southern Ocean and in all of the regions as well. Unlike total precipitation, there is similar interannual variability in Southern Ocean rainfall across all reanalyses except for MERRA.

Regionally, JRA-55 has higher rainfall in the Weddell and Bellingshausen/Amundsen Seas and the Indian Ocean sector compared to the other reanalyses, but has a similar magnitude to ERA-Interim in the Pacific Ocean, and produces one of the lowest rainfall amounts in the Ross Sea (Fig. 8). Specifically, in

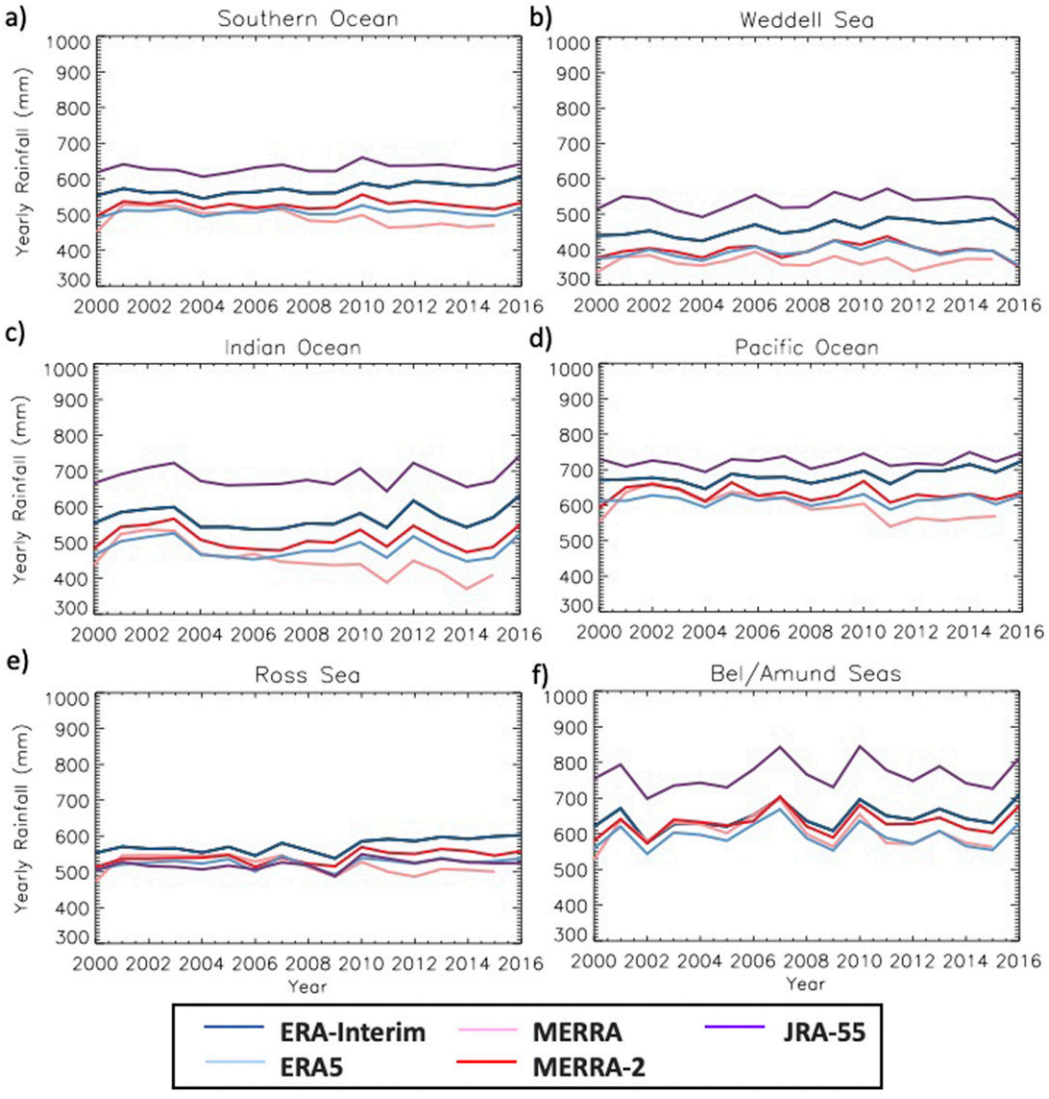

FIG. 8. Annual cumulative rainfall from 2000–16 for the (a) Southern Ocean (entire domain in Fig. 1), (b) Weddell Sea, (c) Indian Ocean, (d) Pacific Ocean, (e) Ross Sea, and (f) Bellingshausen/Amundsen Seas. Note that the *y* axis does not start at zero.

the Ross Sea, ERA-Interim produces the highest rainfall, while JRA-55 in some years has the lowest rainfall of all the products. Also in this region, the spread between the reanalyses is smallest at approximately 50 mm yr^{-1} (Table 4). In the Bellingshausen/Amundsen Seas, ERA-Interim has roughly the same magnitude as MERRA, MERRA-2 and ERA5, all of which are about 200 mm yr^{-1} lower than JRA-55 (Table 4). The largest rainfall amounts are seen in the Bellingshausen/Amundsen Seas, with the lowest in the Weddell Sea. It is important to consider, however, that the majority of the rainfall in

TABLE 4. Average 2000–10 annual rainfall and interannual standard deviations (in parentheses) for each reanalysis. The regions are outlined in Fig. 1. All values in the table are in millimeters.

	Southern Ocean	Weddell Sea	Indian Ocean	Pacific Ocean	Ross Sea	Bellingshausen/Amundsen Seas
ERA-Interim	564.0 (11.2)	511.5 (14.6)	479.1 (20.6)	627.9 (15.7)	596.7 (17.7)	727.5 (34.6)
ERA5	507.6 (10.8)	463.8 (14.8)	383.2 (21.4)	55.7 (13.9)	560.7 (20.0)	695.7 (33.6)
MERRA	502.9 (23.4)	434.9 (18.4)	375.2 (31.6)	557.5 (29.6)	570.0 (29.5)	716.2 (48.0)
MERRA-2	526.3 (15.6)	474.3 (15.8)	404.6 (26.3)	578.6 (24.3)	574.1 (19.9)	733.7 (39.0)
JRA-55	628.4 (14.5)	604.9 (19.1)	574.2 (20.5)	650.6 (16.1)	555.0 (17.9)	894.9 (44.4)

all of the regions is occurring at lower latitudes and not necessarily over the sea ice pack.

c. Frequency of precipitation

Along with the amount, it is also important to understand how often it precipitates in the Southern Ocean, and specifically if the number of days of snowfall and rainfall are changing. Each day that precipitation is greater than zero is counted as a precipitation day in this analysis. According to the reanalyses, precipitation occurs nearly every day of the year across the Southern Ocean (Fig. 9). However, there are some discrepancies between the products. For example, in the Weddell Sea near the Antarctic Peninsula and Ronne Ice Shelf, CFSR, JRA-55, NOAA CIRES, ERA-Interim, and ERA5 show precipitation occurring on average around 340 days or less, while NCEP-R2, MERRA, and MERRA-2 produce precipitation nearly every day. This similar situation also occurs in the Ross Sea near the Ross Ice Shelf, and close to the East Antarctica coastline (Fig. 9). Thus, it makes sense that the largest differences in the precipitation days between the reanalyses occurs in the Weddell and Ross embayments, closest to the continents. Small deviations occur away from the Antarctic continent because nearly all reanalyses produce daily precipitation. Over the whole Southern Ocean, ERA-Interim, followed by CFSR, have the smallest precipitation frequency while MERRA, MERRA-2, and NCEP R2 produce precipitation every day of the year on average.

Similar to what was found in the Arctic Ocean reanalysis comparison (Boisvert et al. 2018), reanalyses are producing precipitation nearly every day over the polar oceans, which is suspected to be too frequent. It is interesting to note that ERA-Interim and ERA5 do not have the same amount of precipitation frequency, whereas MERRA and MERRA-2 precipitate on a daily basis in the Southern Ocean.

d. Frequency of snowfall and rainfall

Similar to total precipitation, snowfall is indicated nearly every day of the year over areas closest to the Antarctic continent. At latitudes around 60°S, the snowfall frequency decreases rapidly where temperatures are warmer (Fig. 10). ERA5 produces snowfall at the lowest latitudes at roughly 50°S, and JRA-55 stops producing snowfall at the highest latitudes, ~60°S. The location of where there are no snowfall days and the gradient over which this transition occurs vary between each of the five reanalyses, and explains the high spread between the products around the latitudinal band of ~60°S. ERA-Interim produces snowfall least frequently, followed by JRA-55. MERRA, MERRA-2, and ERA5 have the highest number of snowfall days. The number of days that each reanalysis produces rainfall is opposite to the snowfall, where the most frequent rainfall occurs at lower latitudes, and decreases slightly to finally almost no days with rainfall closest to the Antarctic continent (Fig. 10). ERA-Interim produces the most frequent rainfall closest to the continent, but MERRA, MERRA-2, and JRA-55 have the most frequent rainfall at lower latitudes. ERA5 has the fewest rainfall days at lower latitudes. The differences between the reanalyses rainfall days again occur at about 60°S latitude, where the transition from rain to snow takes place, and varies depending on the reanalysis.

There is no significant change in the total number of snowfall (not shown) and rainfall (Fig. 11) days between 2000 and 2016. Thus, the magnitude of the rainfall events is increasing since the number of days remains constant in these particular reanalyses. From Fig. 11, each reanalysis shows similar interannual variability in the number of rainfall days except for ERA5. ERA5 has the lowest number of rainfall days for the entire Southern Ocean as well as in every region. JRA-55 has the most amount of rainfall days in all regions except for the Ross Sea. The number of rainfall days for ERA-Interim and MERRA are very similar in all regions and MERRA-2 tends to have slightly fewer rainfall days (roughly 10–20 days) than in MERRA. The Bellingshausen/Amundsen Seas have the most frequent rainfall occurrences, and the Pacific Ocean has the least frequent rainfall occurrences compared to the other regions (Fig. 11).

e. Spurious precipitation

Precipitation frequency varies across the Southern Ocean, but it is unlikely to precipitate every day over large regions. In situ measurements of precipitation taken from ship cruises in the Bellingshausen Sea have showed that some form of precipitation occurred nearly every day and agreed well with the chosen ECMWF reanalysis (Leonard and Cullather 2008; Leonard and Maksym 2011). These results suggest that although measurable precipitation did not occur every day, precipitation is very frequent. One caveat of these studies is that they are limited both spatially and temporally and might not be truly representative of the Southern Ocean as a whole. Ellis et al. (2009) have compared ship- and ground-based measurements of precipitation with *CloudSat* over the global oceans and found good agreement with these observations when *CloudSat* detected precipitation and demonstrated that detectable precipitation is likely not occurring every day. Other simulations have shown an overestimate of small amounts of precipitation when compared with satellite observations (Franklin et al. 2013; Catto et al. 2013). We thus assume that this spurious precipitation occurs within the reanalyses that does not occur in reality, as they demonstrate that it precipitates nearly every day (Fig. 9). This is similar to what was found in the precipitation products in the Arctic Ocean (e.g., Boisvert et al. 2018), where some reanalyses indicate some form of precipitation every day. This spurious precipitation is classified here as any day when the precipitation is less than 0.2 mm day^{-1}. This follows the World Meteorological Organization (WMO) definition of trace precipitation as anything between 0.1–0.2 mm day^{-1} depending on the measurement instruments accuracy and the American Meteorological Society (AMS) definition as 0.01 in. day^{-1}, which is equivalent to 0.254 mm day^{-1}. This spurious precipitation occurs in every reanalysis used in this comparison. Figure 12 shows the annual averaged 2000–10 amount of spurious precipitation and Fig. 13 shows the annual averaged 2000–10 number of spurious precipitation days each year.

All of the reanalyses, with the exception of NCEP-R2, agree that this precipitation mainly occurs near the continent and

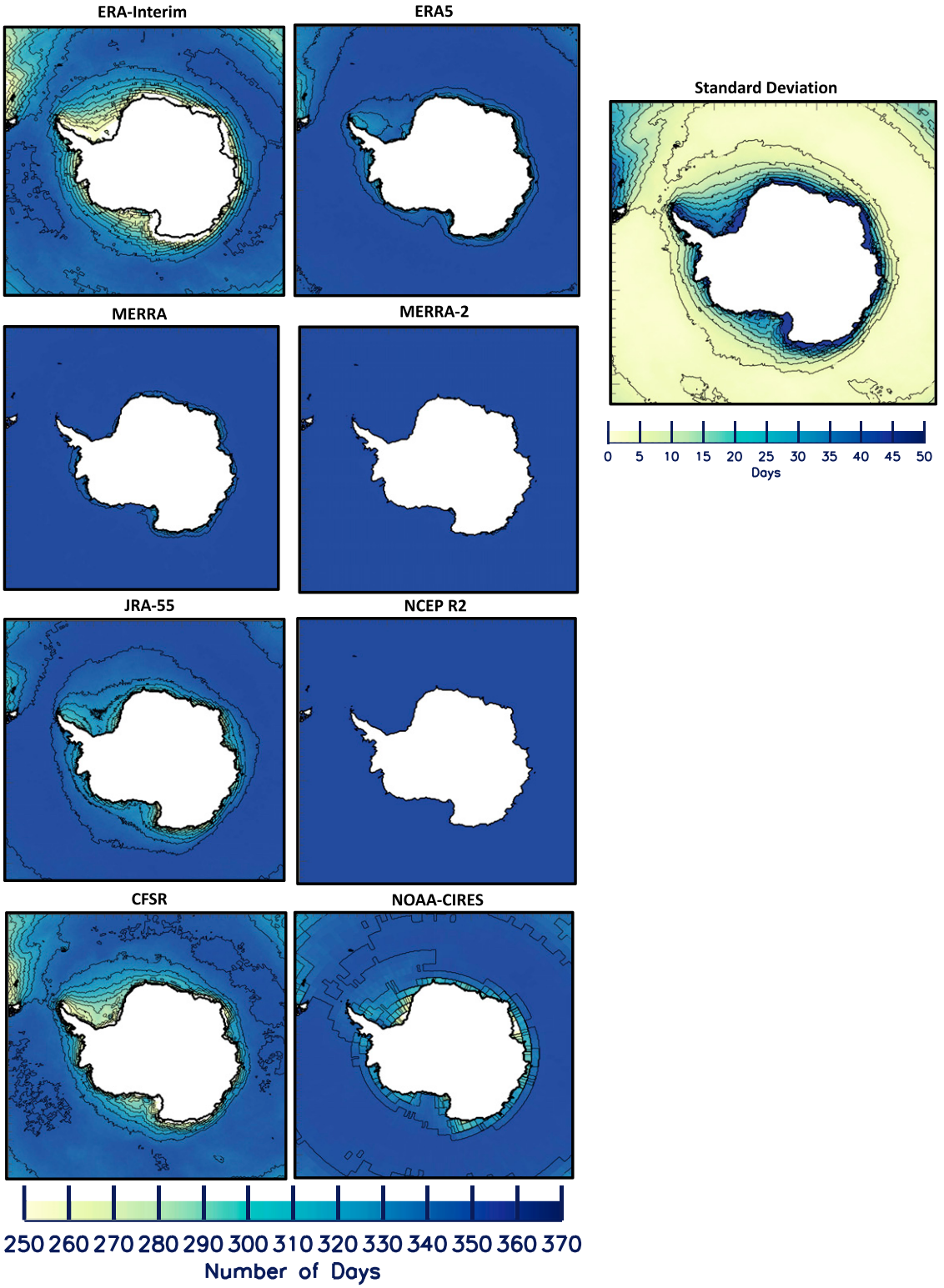

FIG. 9. Average 2000–10 number of days within a year during which precipitation (either snowfall or rainfall) occurs. The standard deviation (mm) is shown on the right. Contour lines in the figures represent the contour lines on the color bars.

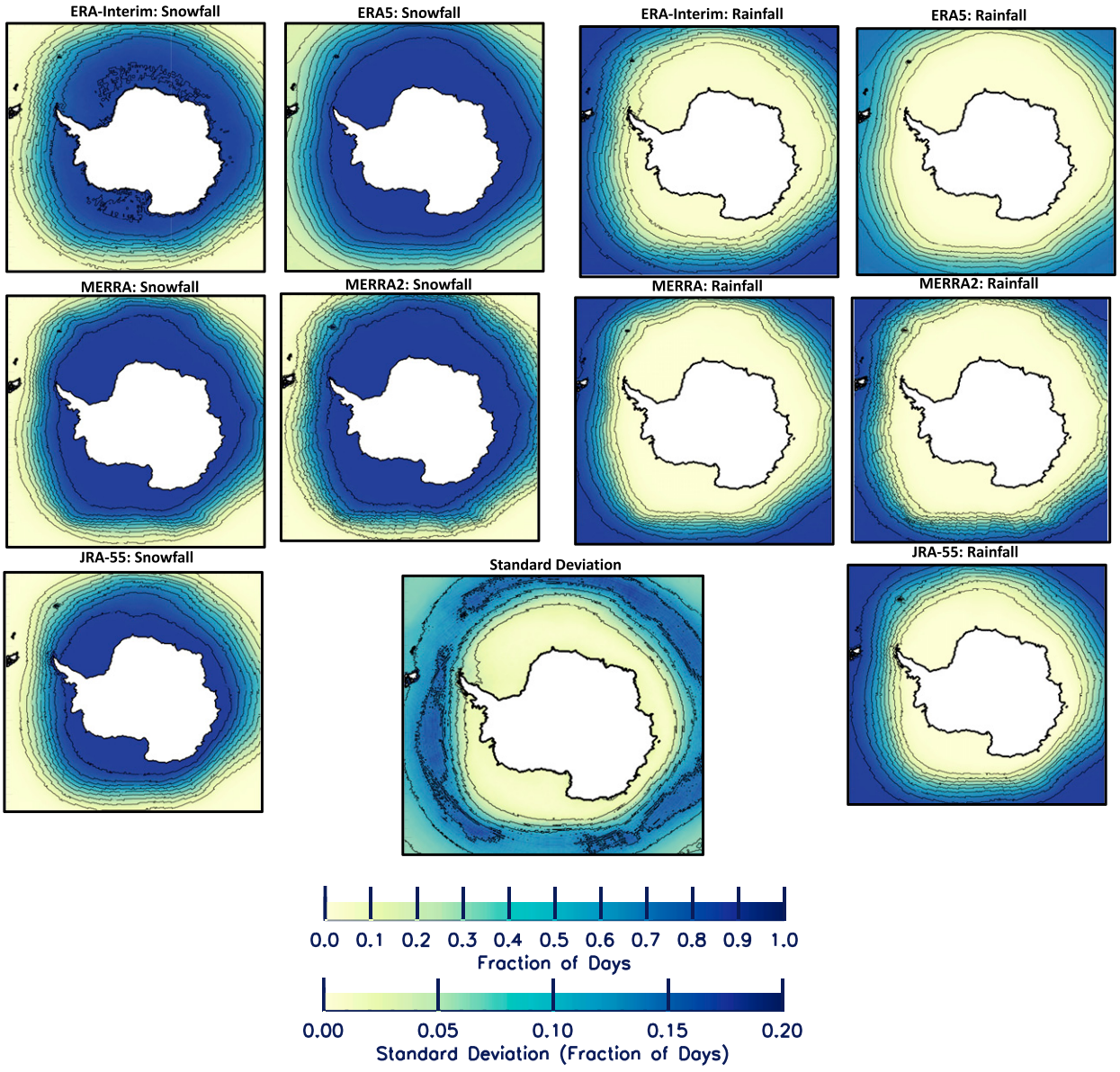

FIG. 10. Average 2000–10 fraction of the number of days within a year during which (left) snowfall and (right) rainfall occurs. The standard deviation is shown on the bottom in fraction of days. Contour lines in the figures represent the contour lines on the color bars.

decreases toward lower latitudes (Fig. 12). Most spurious precipitation is produced in the Weddell, Ross, and Bellingshausen/Amundsen Seas and accumulates to 7.5 mm yr^{-1} on average. MERRA-2 and ERA5 have the most spurious precipitation in the Ross Sea near the Ross Ice Shelf, which is not indicated in the other reanalyses (Fig. 12). Conversely, NCEP-R2 has the least amount of spurious precipitation in close proximity to the Antarctic continent. The largest standard deviations of about 3 mm yr^{-1} occur near to the Antarctic continent and decrease to about 1 mm yr^{-1} near 55°S. Overall, the reanalyses, except NCEP-R2, have similar patterns in both the frequency and amount of spurious precipitation in the Southern Ocean; however, the exact frequency and amount differ. Spurious precipitation, defined in this study, amounts to around 0.75% of the total precipitation over the Southern Ocean in the reanalyses (Fig. 12).

From Fig. 13, it is apparent that NCEP-R2 produces spurious precipitation most frequently in the Southern Ocean, approximately 100 days yr^{-1}. CFSR produces this least frequently, with the other reanalyses falling in between NOAA CIRES and NCEP-R2. The most frequent spurious precipitation in all of the reanalyses besides NCEP-R2 occurs in the Weddell, Ross and Bellingshausen/Amundsen Seas at about 120 days yr^{-1}. The least amount of spurious precipitation occurs in the cyclone belt near 55°–65°S latitudes off the coast of East Antarctica.

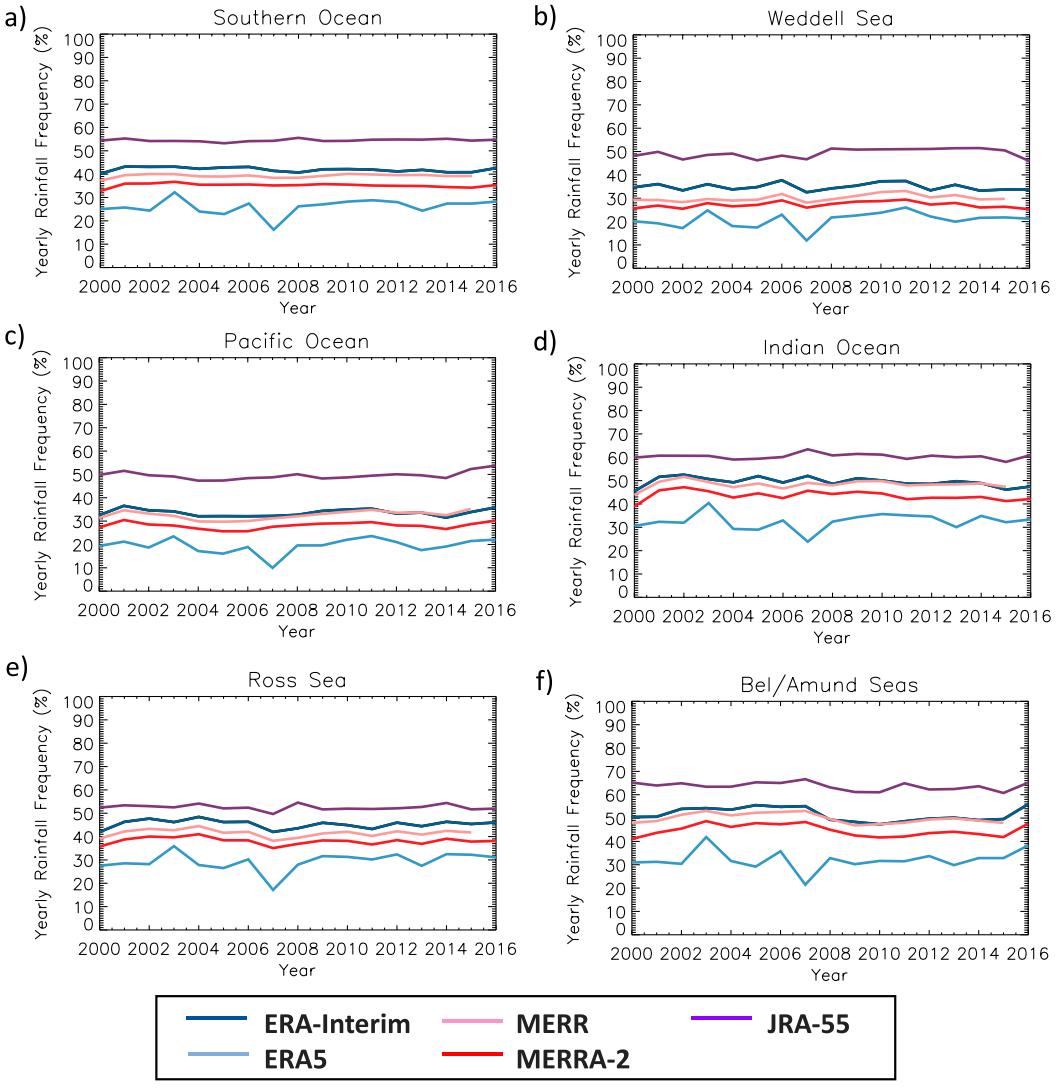

FIG. 11. Frequency of the annual number of days of rainfall to the number of days of precipitation from 2000–16 for the (a) Southern Ocean (entire domain in Fig. 1), (b) Weddell Sea, (c) Indian Ocean, (d) Pacific Ocean, (e) Ross Sea, and (f) Bellingshausen/Amundsen Seas.

f. Comparisons with buoy data

Figure 14 shows the time series of the snow depth from the 2014S9 buoy along with snowfall and rainfall rates from five reanalyses. A snowfall event recorded by the buoy is denoted by a black dotted vertical line and any day that the hourly air temperature recorded by the buoy was above freezing (>0°C) is denoted by a red dotted vertical line. This particular buoy was deployed on 5 February 2014 at the end of the austral summer, beginning with a snow depth of ~10 cm. Snow depth increased throughout the fall and winter months to a maximum depth of ~50 cm. Snow depth was reduced in the following summer due to melt and melt associated with rain events, losing ~20 cm of snow, but then rapidly increased in thickness in the fall/winter, reaching ~60 cm. From this figure, it is apparent that the snowpack around this buoy is very dynamic and there are multiple "events" where the snow depth increases. The reanalyses produce multiple snowfall events at the 2014S9 snow buoy location throughout its lifetime and consistently produce snowfall events on the same days. However, the magnitudes of these events have a spread of ~10 mm day^{-1} between the reanalyses (Fig. 14). There are also times when all reanalyses produce a large snowfall event (see Fig. S2, with rates between 5–20 mm day^{-1}), but no change or only minimal change in buoy snow depth occurs (e.g., ~day 260; Fig. S2). At these times, a snowfall event may have occurred but the snow may have been redistributed by wind or lost to leads. At other times, (e.g., day 290), large precipitation rates occur and the snow depth also increases by 20 cm. During these events, there is a clear relationship between snowfall and snow accumulation recorded by the buoy; however, the rate of snowfall might not correspond to the amount of newly accumulated snow. It is

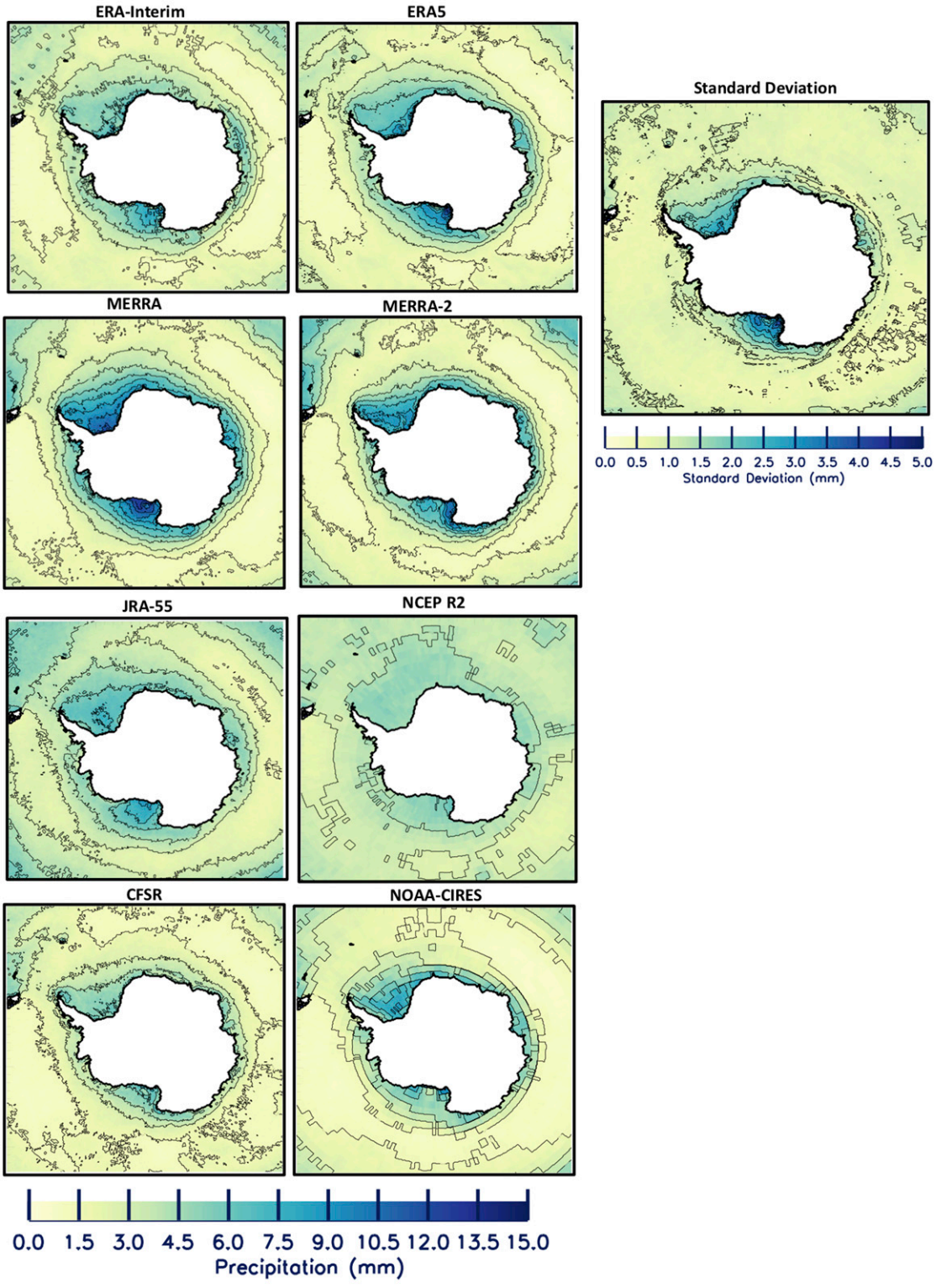

FIG. 12. (a) Average 2000–10 annual cumulative spurious precipitation along with the standard deviation between products (mm). Spurious precipitation is classified as any type of precipitation with rates less than 0.2 mm day^{-1}. Contours are on the color bars.

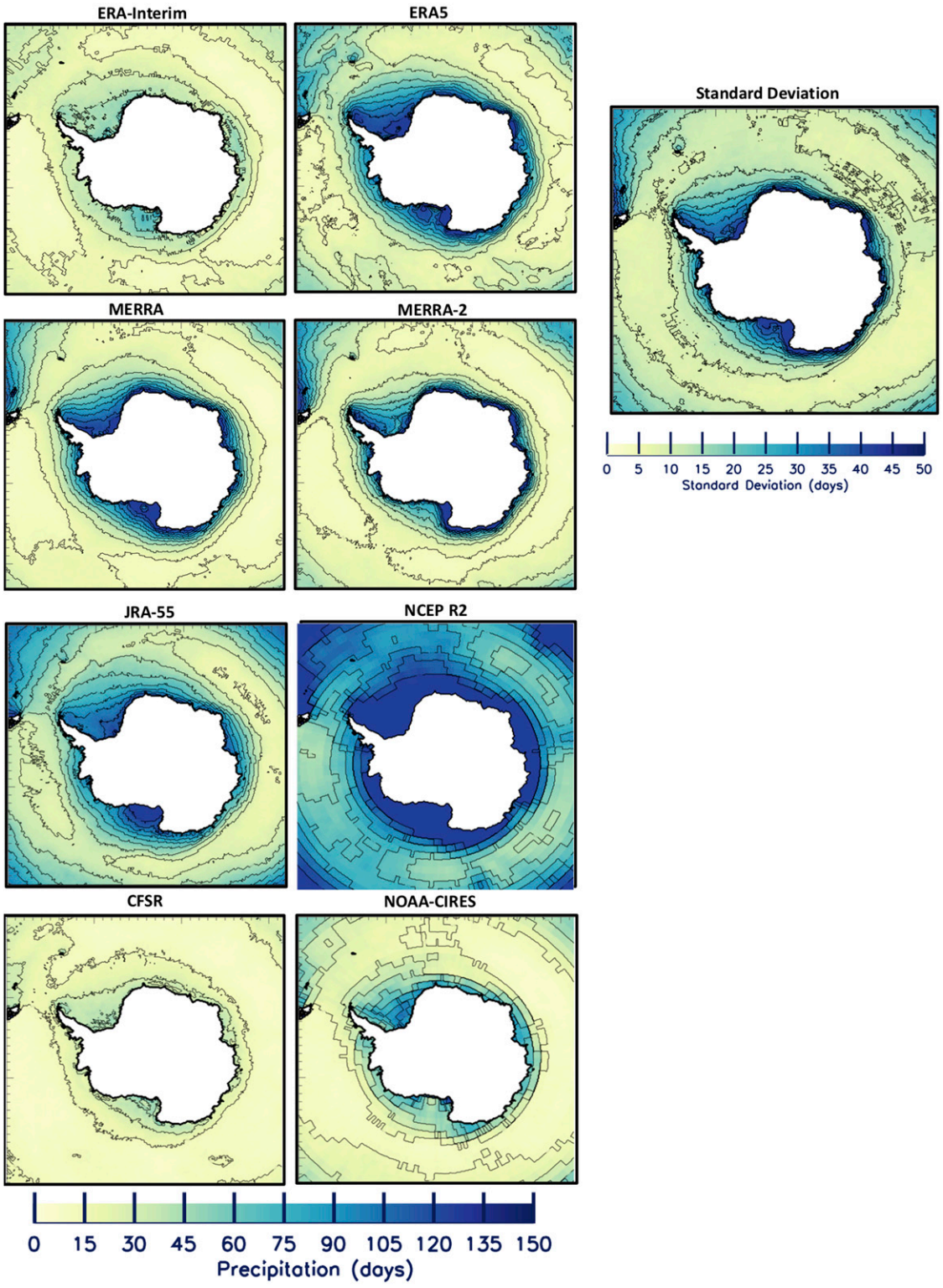

FIG. 13. Average 2000–10 annual spurious precipitation days along with the standard deviation between products in days. Spurious precipitation is classified as any type of precipitation with rates less than 0.2 mm day^{-1}. Contours are on the color bars.

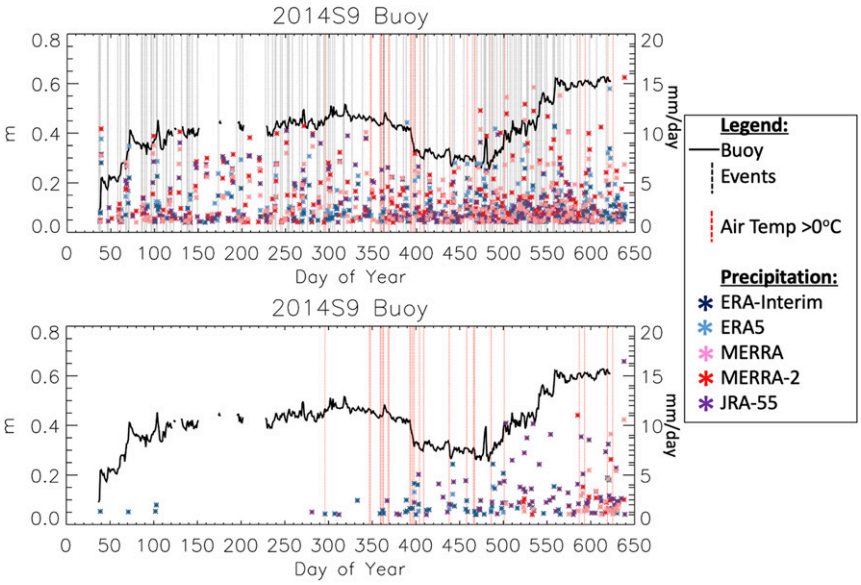

FIG. 14. (a) Snowfall without precipitation < 1 mm day^{-1} included from five reanalyses for the 2014S9 Antarctic snow buoy. (b) Rainfall from five reanalyses without precipitation < 1 mm day^{-1} included for the 2014S9 snow buoy. The snow depth (m) recorded by the buoy is the black line. Each colored asterisk shows the precipitation rate (mm day^{-1}) for that respective reanalyses at the location of the buoy. The black vertical dotted lines signify an "event" when the snow depth increases by 1 cm or more in a day. The red vertical dotted lines signify any hour of the day when the air temperature is >0°C.

also important to note that like the Arctic Ocean, reanalyses are producing precipitation nearly every day at the buoy location (Fig. S2a).

The air temperature recorded at the snow buoys can be used to evaluate the phase of precipitation events from reanalyses. For example, snow buoy 2014S9 in Fig. 14b shows times when the air temperatures are above freezing coincident with when reanalysis rainfall occurs. During the summer months whenever the air temperature is above freezing, the reanalyses produce rainfall in nearly every occurrence except for a few days. The warmer air temperatures do not always dictate rain however, but are often associated with melt events, which coincide with a decrease in snow depth. ERA-Interim produces some rainfall from days 50 to 100 (~March) when the air temperatures are below freezing. ERA-Interim was shown to produce too many rainfall events compared to the other reanalyses in the Arctic Ocean (e.g., Boisvert et al. 2018). At this snow buoy's location, ERA-Interim has the most rainfall events, followed by JRA-55, then ERA5 and MERRA. Surprisingly, MERRA-2 does not produce any rainfall events. The largest warm event during days 387–400 (22 January–4 February 2015) also has rainfall events and a large decrease in the snowpack ~10 cm, but some reanalyses also produce snowfall during this period (Fig. 14a). Regardless, the rain-on-snow events and warm temperatures substantially reduce the snow depth. Other such warm periods are concurrent with rainfall events.

Interpreting reanalysis precipitation events with coincident changes in snow depth measurements from buoy data is challenging given the uncertainties in the buoy data quality, and not knowing which processes (e.g., dune migration vs snow accumulation) may be influencing snow conditions (Table 5 and Fig. 15). There are a handful of cases (e.g., days ~38, 70, 100, 475, and 550, Fig. 14a) when large increases in snow depth are attributed to large snowfall events in the reanalyses; and when comparing these precipitation events to an increase in snow depth during the winter months (May–September) most of the reanalysis precipitation events show fair agreement with the buoy data (Table 5). Table 6 lists the kappa statistics, or a skill score of how well each of the reanalyses and buoys agree with each other. For buoy data, a wet day was identified when snow depth increased by 1 cm. For reanalysis, a wet day was identified when daily precipitation within 1 day of buoy snowfall was greater than 1 mm. We only focused on the winter months (May–September) and allowed for a ±1-day buffer for when these occurrences matched up. The kappa statistic (κ) is calculated via (1), where p_o is the relative observed agreement between the buoys and the reanalysis and p_e is the probability of random agreement between the buoys and the reanalyses. The terms p_o and p_e are computed from the scenarios (a–d) outlined in Table 6:

$$\kappa = \frac{p_o - p_e}{1 - p_e}, \tag{1}$$

where

$$p_o = \frac{a + d}{a + b + c + d},$$

TABLE 5. Snow buoys and reanalyses skill scores during the kappa statistics using a >1 mm day^{-1} precipitation threshold and a >1 cm day^{-1} change in snow depth from the snow buoys during the winter months (May–September).

Buoy	ERA-Interim	ERA5	MERRA	MERRA-2	JRA-55	NCEP-R2
2013S7	0.48	0.59	0.48	0.64	0.49	0.39
2013S8	0.34	0.29	0.36	0.29	0.33	0.39
2014S10 (2014 winter)	0.45	0.36	0.36	0.43	0.34	0.19
2014S10 (2015 winter)	0.37	0.35	0.31	0.53	0.38	0.32
2014S11	0.31	0.28	0.24	0.48	0.31	0.24
2014S12 (winter 2014)	0.53	0.46	0.47	0.61	0.49	0.32
2014S12 (winter 2015)	0.37	0.35	0.43	0.37	0.36	0.25
2014S9 (winter 2014)	0.38	0.28	0.24	0.49	0.40	0.34
2014S9 (winter 2015)	0.27	0.29	0.32	0.30	0.33	0.33
2016S31	0.40	0.45	—	0.42	0.36	0.32
2016S37	0.36	0.32	—	0.34	0.28	0.15
2016S38	0.26	0.33	—	0.29	0.40	0.26
2016S40	0.40	0.39	—	0.51	0.39	0.17
Average	0.38	0.36	0.36	0.44	0.37	0.28

and

$$p_e = p_{\text{yes}} + p_{\text{no}} = \left(\frac{a+b}{a+b+c+d} \times \frac{a+c}{a+b+c+d}\right) + \left(\frac{c+d}{a+b+c+d} \times \frac{b+d}{a+b+c+d}\right).$$

Overall, all of the reanalyses show a fair agreement with the buoys, except MERRA-2 which shows a moderate agreement. MERRA-2 also had the highest kappa statistic at buoy 2013S7, showing a substantial agreement with the buoy. The average score of "fair" may be due to the higher frequency of melt events, windy conditions, and convergence of the sea ice floes, all factors that can change the snow depth and sometimes can cause no change in snow depth when precipitation occurs or cause a change in snow depth when no precipitation occurs (Massom et al. 2001; Sturm and Massom 2017), as well as to large uncertainties in the buoy data.

The magnitude of the precipitation events is a much more difficult quantity to assess. This is because of snow compaction over time and snow redistributions due to both winds and sea

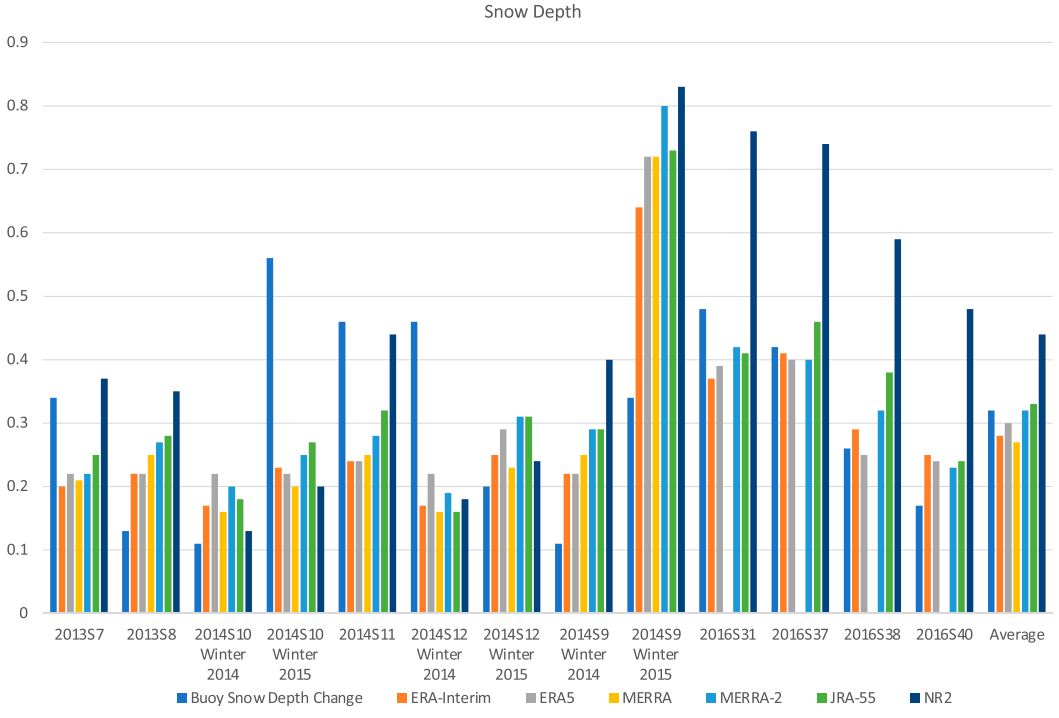

FIG. 15. The snow depth increase at each buoy over the winter (May–September) in dark blue. The snow depth equivalent from the total precipitation at each buoy location over the winter (May–September) for each reanalysis. Precipitation amounts are converted into snow depth using the average Antarctic sea ice wintertime snow density of 350 kg m^{-3} from Maksym and Markus (2008). All values are in meters.

TABLE 6. Kappa statistic scenarios and skill score classification. The kappa statistic uses four different scenarios: the number of occurrences when both the reanalysis precipitation was >1 mm and change in buoy snow depth >1 cm (denoted *a*), the reanalysis precipitation was >1 mm and there was no change to the buoy snow depth (denoted *b*), no reanalysis precipitation occurred and the buoy snow depth change was >1 cm (denoted *c*), and no reanalysis precipitation occurred and there was no change in buoy snow depth (denoted *d*).

		Reanalysis		
		Yes	No	Kappa skill score
Buoy	Yes	*a*	*b*	$\kappa \leq 0$ no agreement
		Precipitation > 1 mm;	Precipitation < 1 mm;	$0.1 < \kappa \leq 0.2$ none to slight
		Δ snow depth > 1 cm	Δ snow depth >1 cm	$0.21 < \kappa \leq 0.4$ fair
	No	*c*	*d*	$0.41 < \kappa \leq 0.6$ moderate
		Precipitation > 1 mm;	Precipitation < 1 mm;	$0.61 < \kappa \leq 0.8$ substantial
		Δ snow depth = 0	Δ snow depth = 0	$0.81 < \kappa \leq 1.0$ almost perfect

ice dynamics. Figure 15 shows the change in snow depth (the difference between the largest and smallest snow amounts) from each buoy during the winter months (May–September) and the snow depth equivalent of the total precipitation at each buoy over the winter (May–September) using only precipitation $> 1\,\text{mm day}^{-1}$. Precipitation amounts are transferred into snow depth using the average wintertime Antarctic sea ice snow density of $350\,\text{kg m}^{-3}$ from Maksym and Markus (2008). From Fig. 15, the amount of snow depth change at the buoys are different from the amount of reanalyses equivalent snow depth derived from precipitation. The reanalyses equivalent snow depths derived from precipitation rates are not consistently higher than the buoy snow depth. For example, the 2014S12 winter 2014 and 2014S10 winter 2015 buoy snow depth change was much larger than the reanalyses equivalent snow depth, the 2013S8 and 2014S9 winter 2014 buoy snow depth was much lower than the reanalyses equivalent snow depth, and other buoys like the 2016S37 have similar snow depths to the reanalyses equivalent snow depth. This further complicates trying to discern precipitation amounts and snow depth changes measured by a buoy. When looking at the average snow depth change from the buoys and the average equivalent snow depth from the reanalyses precipitation it appears that the equivalent snow depths are consistent with the buoys. On average, MERRA-2 produces nearly identical amounts, with NCEP-R2 always consistently higher. However, no definitive assumptions can be made about the magnitude of the precipitation events from the reanalyses due to all of the complex processes that occur once the precipitation reaches the surface. This also highlights the challenge of interpreting these buoy "point" measurements with the much larger spatial scales of the reanalyses precipitation products. Autonomous systems that can monitor the spatial variability in snow depth across larger areas (Nicolaus et al. 2017), combined with precipitation sensors (Leonard and Cullather 2008) and technological advancements of remote sensing capabilities will likely be a path forward in better measuring and monitoring precipitation at high latitudes.

4. Discussion and conclusions

Our results have shown that precipitation from reanalyses over the Southern Ocean tends to agree in the spatial patterns and interannual variability, but the magnitude of the annual precipitation varies between individual products. In the Southern Ocean, as in the Arctic Ocean (Boisvert et al. 2018), CFSR produces the highest precipitation and ERA-Interim produces too little snowfall and JRA-55 produces too much rainfall when compared to the other products. In the Southern Ocean, the same spatial precipitation patterns exist between *CloudSat*-derived monthly snowfall and the reanalyses' snowfall, providing confidence that the spatial precipitation patterns from reanalyses are reliable. Spatial patterns of precipitation from this analysis are also similar to previous Southern Ocean precipitation studies like Legates (1995) and Bromwich et al. (2011), with less precipitation occurring in the Weddell Sea and more away from the continent.

All reanalyses produce the least amount of precipitation in the southern Ross and Weddell Seas in embayments near the ice shelves. In these areas, persistent cold dry katabatic winds blow from the continent, across the ice shelves and out over the sea ice (Parish and Bromwich 2007). These cold dry winds are not conducive for the formation of precipitation, and thus less precipitation occurs in these regions. These areas are also shielded from eastward-traversing synoptic systems by topography. All reanalyses also produce the highest precipitation off the coasts of East Antarctica in the Indian and Pacific Ocean regions. Reanalyses and *CloudSat* also indicate more precipitation amounts west of the Antarctic Peninsula and less precipitation on the eastern side. This is likely caused by more persistent storms and weather generally moving eastward from the Bellingshausen/Amundsen Seas into the Weddell Sea, resulting in orographic forcing along the windward side of the peninsula (Parish 1983; Turner et al. 1995).

The spatial patterns of low and high precipitation amounts also compare with the distribution of cyclones (Uotila et al. 2011; Papritz et al. 2014). Large precipitation amounts occur where the largest number of cyclones occur (Uotila et al. 2011; Papritz et al. 2014). These tend to be located off the coasts of eastern Antarctica (in the eastern Ross Sea region, and off the coasts in the Pacific and Indian Ocean regions, where the largest spread between the reanalysis precipitation occurs. As cyclones are most prevalent in these areas, the precipitation amounts during these cyclones could be widely variable between the reanalyses because the precipitation rates are dependent on their respective cloud microphysics and precipitation schemes (Han et al. 2013). The smallest differences between reanalyses occur in the Weddell and Ross Seas in areas where the least amount of cumulative precipitation is

produced. In these areas the smallest number of cyclones are also detected (Uotila et al. 2011; Papritz et al. 2014). It appears that the reanalyses are getting the location and hence precipitation of where the cyclones are occurring correctly, but perhaps not the magnitude of the precipitation given that the deviations between reanalyses are large.

Reanalyses disagree on the magnitude of snowfall and rainfall in the Southern Ocean, and this is especially apparent at lower latitudes where temperatures are warmer, and the phase of the precipitation is handled differently by each reanalyses microphysical scheme (refer to references in Table 1). This is also apparent with the comparisons from *CloudSat*. Overall, ERA-Interim produced the least amount of snowfall and JRA-55 produced the most amount of rainfall in the Southern Ocean. Our analysis has also shown that precipitation is being produced nearly every day in the Southern Ocean, like in the Arctic Ocean. Often, the amount is less than 0.2 mm day^{-1}, which we define in this analysis as spurious precipitation. Spurious precipitation occurs on average about 60 days yr^{-1} and accounts for roughly 4.5 mm of annual precipitation in the Southern Ocean.

Comparing wintertime snow buoy measurements with the reanalysis precipitation, using the kappa statistic, shows fair agreement that the reanalyses are producing precipitating events when the buoy sees an increase in snow depth; however, the spread of the precipitation rates during these events remains large. The precipitation rate that the reanalyses produce are dependent on many factors, here we name a few: 1) the representation of the sea ice as it affects exchanges of heat, moisture, and momentum and thus alters the boundary layer; 2) the amount of moisture and the temperature of the atmosphere, along with how each treat aerosols, affect the amount of clouds produced and cloud microphysics therein; 3) their respective cloud microphysics schemes, however simple or complex, that determine the precipitation rate and phase (see Table 1); and 4) their specific assimilated observational datasets and data assimilation schemes.

A specific issue is the differences occurring in subsequent iterations of reanalyses, which have typically undergone extensive changes in resolution, model components, and the data assimilation system. The attribution of changes in precipitation amount and character from one version to the next may not be straightforward. The update from MERRA to MERRA-2 involved a transition in the model grid to the cubed sphere and the elimination of high-latitude Cartesian grid filtering. Additionally, significant changes to the cloud microphysics were made (Molod et al. 2015). As compared to ERA-I, the ERA5 employed an updated representation of high-latitude mixed-phase clouds and prognostic variables for precipitating rain and snow (Forbes et al. 2011; Hersbach et al. 2020). Both systems apply different sea ice and SST boundary conditions, which may affect the local atmosphere/ocean moisture exchange. Additionally, both systems conserve global dry air mass in their more recent versions (Takacs et al. 2016).

Precipitation in the Southern Ocean remains difficult to evaluate. Possible reasons for this include the following:

1) High uncertainty of precipitation amounts and phase of precipitation, which is in large part due to a severe lack of in situ measurements.
2) High uncertainty in understanding the cloud processes and microphysics over the Southern Ocean (Pope et al. 2017).
3) Difficulty in using buoy snow depth data for precipitation evaluation, exacerbated by the Antarctic sea ice and environment, which leads to more complex processes affecting the snowpack once precipitation falls on the sea ice (Massom et al. 2001; Webster et al. 2018).

Currently it is difficult to assess which reanalysis precipitation product is the most accurate due to the lack of in situ observations of precipitation and other variables in the remote locations of the Southern Ocean, and the difficulty of modeling cloud microphysics in this region where little is known. Our results cannot pinpoint the accuracy of one reanalysis over the other, but show that the reanalysis products produce similar spatial patterns and annual cycles, precipitate too frequently (e.g., spurious precipitation), and are decent at reproducing precipitation events when compared to snow buoys in the Weddell Sea in the winter.

A better understanding of precipitation in the Southern Ocean is necessary and becomes especially important in a warming climate, where precipitation amount, phase, and patterns are expected to change considerably (Trenberth 2011). Thus, understanding reanalysis precipitation products along with their discrepancies, and the sources of their discrepancies, is that much more important for understanding how these changes will affect the sea ice climate system in the future. More work must be undertaken to better understand, and to model precipitation for an improved understanding of the snowpack and snowpack evolution on Antarctic sea ice, as well as to improve our understanding of the hydrologic cycle in the Southern Ocean. Specifically, more in situ observations of precipitation and processes therein are needed over the Southern Ocean, which can then be utilized to improve precipitation schemes in reanalyses as well as in deriving satellite precipitation rates.

Acknowledgments. The NCEP R1 and NCEP R2 were obtained from the NCAR Research Data Archive. CFSR fields were obtained from the National Operational Model Archive and Distribution System (NOMADS) at the U.S. National Climatic Data Center. ERA-Interim and ERA-5 fields were obtained from the ECMWF Meteorological Archival and Retrieval System (MARS). JRA-55 fields were obtained from the Japan Meteorological Agency Climate Prediction Division, Global Environment and Marine Department. MERRA and MERRA-2 were obtained from the NASA Goddard Earth Sciences Data and Information Services Center (GES-DISC). Snow buoy data were obtained from www.meereisportal.de. The Authors thank Dr. Tristian L'Ecuyer for providing the C-SNOW-PROFILE (2C-SNOW) *CloudSat* product.

The work of L. Boisvert, M. Webster, A. Petty, and T. Markus was funded by the NASA-ESA Snow on Sea Ice (NESOSI) project. R. Cullather is funded through a grant from the NASA Modeling, Analysis, and Prediction (MAP) Program. D. Bromwich is funded through NSF Grant 1823135 and Contribution 1599 of Byrd Polar and Climate Research Center. This work is done as part of the ISSI Antarctic Sea Ice Working Group.

REFERENCES

Adam, J. C., and D. P. Lettenmaier, 2003: Adjustment of global gridded precipitation for systematic bias. *J. Geophys. Res.*, **108**, 4257, https://doi.org/10.1029/2002JD002499.

Bacmeister, J. T., M. J. Suarez, and F. R. Robertson, 2006: Rain reevaporation, boundary layer–convection interactions, and Pacific rainfall patterns in the AGCM. *J. Atmos. Sci*, **63**, 3383–3403, https://doi.org/10.1175/JAS3791.1.

Bauer, P., A. Thorpe, and G. Brunet, 2015: The quiet revolution of numerical weather prediction. *Nature*, **525**, 47–55, https://doi.org/10.1038/nature14956.

Behrangi, A., and M. Richardson, 2018: Observed high-latitude precipitation amount and pattern and CMIP5 model projections. *Remote Sens.*, **10**, 1583, https://doi.org/10.3390/rs10101583.

——, M. Lebsock, S. Wong, and B. Lambrigtsen, 2012: On the quantification of oceanic rainfall using spaceborne sensors. *J. Geophys. Res.*, **117**, D20105, https://doi.org/10.1029/2012JD017979.

——, G. Stephens, R. F. Adler, G. J. Huffman, B. Lambrigsten, and M. Lebsock, 2014: An update on the oceanic precipitation rate and its zonal distribution in light of advanced observations from space. *J. Climate*, **27**, 3957–3965, https://doi.org/10.1175/JCLI-D-13-00679.1.

Boisvert, L. N., M. A. Webster, A. A. Petty, T. Markus, D. H. Bromwich, and R. I. Cullather, 2018: Intercomparison of precipitation estimates over the Arctic Ocean and its peripheral seas from reanalyses. *J. Climate*, **31**, 8441–8462, https://doi.org/10.1175/JCLI-D-18-0125.1.

Bosilovich, M. G., F. R. Robertson, and J. Chen, 2011: Global energy and water budgets in MERRA. *J. Climate*, **24**, 5721–5739, https://doi.org/10.1175/2011JCLI4175.1.

Bromwich, D. H., 1988: Snowfall in high southern latitudes. *Rev. Geophys.*, **26**, 149–168, https://doi.org/10.1029/RG026i001p00149.

——, B. Chen, and R. Y. Tzeng, 1995: Arctic and Antarctic precipitation simulations produced by the NCAR community climate models. *Ann. Glaciol.*, **21**, 117–122, https://doi.org/10.3189/S026030550001569X.

——, J. P. Nicolas, and A. J. Monaghan, 2011: An assessment of precipitation changes over Antarctica and the Southern Ocean since 1989 in contemporary global reanalyses. *J. Climate*, **24**, 4189–4209, https://doi.org/10.1175/2011JCLI4074.1.

——, and Coauthors, 2012: Tropospheric clouds in Antarctica. *Rev. Geophys.*, **50**, RG1004, https://doi.org/10.1029/2011RG000363.

Catto, J. L., C. Jakob, and N. Nicholls, 2013: A global evaluation of fronts and precipitation in the ACCESS model. *Aust. Meteor. Oceanogr. J.*, **63**, 191–203, https://doi.org/10.22499/2.6301.012.

Cohen, J., and Coauthors, 2014: Recent Arctic amplification and extreme mid-latitude weather. *Nat. Geosci.*, **7**, 627–637, https://doi.org/10.1038/ngeo2234.

Compo, G. P., and Coauthors, 2009: NOAA CIRES Twentieth Century Global Reanalysis version 2. Research Data Archive at the National Center for Atmospheric Research, Computational and Information Systems Laboratory, accessed November 2018, https://doi.org/10.5065/D6QR4V37.

——, and Coauthors, 2011: The Twentieth Century Reanalysis Project. *Quart. J. Roy. Meteor. Soc.*, **137**, 1–28, https://doi.org/10.1002/QJ.776.

Cullather, R. I., and M. G. Bosilovich, 2011: The moisture budget of the polar atmosphere in MERRA. *J. Climate*, **24**, 2861–2879, https://doi.org/10.1175/2010JCLI4090.1.

Dai, A., 2006: Precipitation characteristics in eighteen coupled climate models. *J. Climate*, **19**, 4605–4630, https://doi.org/10.1175/JCLI3884.1.

Dee, D. P., and Coauthors, 2011: The ERA-Interim reanalysis: Configuration and performance of the data assimilation system. *Quart. J. Roy. Meteor. Soc.*, **137**, 553–597, https://doi.org/10.1002/qj.828.

de Lavergne, C., J. B. Palter, E. D. Galbraith, R. Bernardello, and I. Marinov, 2014: Cessation of deep convection in the open Southern Ocean under anthropogenic climate change. *Nat. Climate Change*, **4**, 278–282, https://doi.org/10.1038/nclimate2132.

Durack, P. J., S. E. Wijffels, and R. J. Matear, 2012: Ocean salinities reveal strong global water cycle intensification during 1950 to 2000. *Science*, **336**, 455–458, https://doi.org/10.1126/science.1212222.

Ellis, T. D., T. L'Ecuyer, J. M. Haynes, and G. L. Stephens, 2009: How often does it rain over the global oceans? The perspective from CloudSat. *Geophys. Res. Lett.*, **36**, L03815, https://doi.org/10.1029/2008GL036728.

Forbes, R. M., A. M. Tompkins, and A. Untch, 2011: A new prognostic bulk microphysics scheme for the IFS. ECMWF Tech. Memo. 649, European Centre for Medium-Range Weather Forecasts, 28 pp.

Franklin, C. N., Z. Sun, D. Bi, M. Dix, H. Yan, and A. Bodas-Salcedo, 2013: Evaluation of clouds in ACCESS using the satellite simulator package COSP: Global, seasonal, and regional cloud properties. *J. Geophys. Res. Atmos.*, **118**, 732–748, https://doi.org/10.1029/2012JD018469.

Gelaro, R., and Coauthors, 2017: The Modern-Era Retrospective Analysis for Research and Applications, version-2 (MERRA-2). *J. Climate*, **30**, 5419–5454, https://doi.org/10.1175/JCLI-D-16-0758.1.

Giles, K. A., S. W. Laxon, and A. L. Ridout, 2008: Circumpolar thinning of Arctic sea ice following the 2007 record ice extent minimum. *Geophys. Res. Lett.*, **35**, L22502, https://doi.org/10.1029/2008GL035710.

Goodison, B. E., P. Y. T. Louie, and D. Yang, 1998: WMO solid precipitation intercomparison. Instruments and Observing Methods Rep. 67, WMO/TD-872, 212 pp., https://www.wmo.int/pages/prog/www/IMOP/publications/IOM-67-solid-precip/WMOtd872.pdf.

Goosse, H., and V. Zunz, 2014: Decadal trends in the Antarctic sea ice extent ultimately controlled by ice–ocean feedback. *Cryosphere*, **8**, 453–470, https://doi.org/10.5194/tc-8-453-2014.

Grosfeld, K., and Coauthors, 2016: Online sea-ice knowledge and data platform <www.meereisportal.de>. *Polarforschung*, **85**, 143–155, https://doi.org/10.2312/polfor.2016.011.

Grumbine, R. W., 1996: Automated passive microwave sea ice concentration analysis at NCEP, U.S. Dept. Commerce NOAA/NWS/NCEP Tech. Note, OMB Contribution 120, 13 pp.

Han, M., S. A. Braun, T. Matsui, and C. R. Williams, 2013: Evaluation of cloud microphysics schemes in simulations of a winter storm using radar and radiometer measurements. *J. Geophys. Res. Atmos.*, **118**, 1401–1419, https://doi.org/10.1002/JGRD.50115.

Haynes, J. M., T. S. L'Ecuyer, G. L. Stephens, S. D. Miller, C. Mitrescu, N. B. Wood, and S. Tanelli, 2009: Rainfall retrieval over the ocean with spaceborne W-band radar. *J. Geophys. Res.*, **114**, D00A22, https://doi.org/10.1029/2008JD009973.

Hersbach, H., and Coauthors, 2020: The ERA5 global reanalysis: Achieving a detailed record of the climate and weather for the past 70 years. *EGU General Assembly 2020*, Online [no city or country location], EGU2020-10375, https://doi.org/10.5194/EGUSPHERE-EGU2020-10375.

Hirahara, S., M. Ishii, and Y. Fukuda, 2014: Centennial-scale sea surface temperature analysis and its uncertainty. *J. Climate*, **27**, 57–75, https://doi.org/10.1175/JCLI-D-12-00837.1.

Huang, Y., S. T. Siems, M. J. Manton, D. Rosenfeld, R. Marchand, G. M. McFarquhar, and A. Protat, 2016: What is the role of sea

surface temperature in modulating cloud and precipitation properties over the Southern Ocean? *J. Climate*, **29**, 7453–7476, https://doi.org/10.1175/JCLI-D-15-0768.1.

Ishii, M., A. Shouji, S. Sugimoto, and T. Matsumoto, 2005: Objective analyses of sea-surface temperature and marine meteorological variables for the 20th century using ICOADS and the Kobe Collection. *Int. J. Climatol.*, **25**, 865–879, https://doi.org/10.1002/joc.1169.

Kalnay, E., and Coauthors, 1996: The NCEP/NCAR 40-Year Reanalysis Project. *Bull. Amer. Meteor. Soc.*, **77**, 437–471, https://doi.org/10.1175/1520-0477(1996)077<0437:TNYRP>2.0.CO;2.

Kanamitsu, M., W. Ebisuzaki, J. Woollen, S.-K. Yang, J. J. Hnilo, M. Fiorino, and G. L. Potter, 2002: NCEP-DOE AMIP-II Reanalysis (R-2). *Bull. Amer. Meteor. Soc.*, **83**, 1631–1643, https://doi.org/10.1175/BAMS-83-11-1631.

King, J. C., and J. Turner, 1997: *Antarctic Meteorology and Climatology*. Cambridge University Press, 409 pp., https://doi.org/10.1017/CBO9780511524967.

Kobayashi, S., and Coauthors, 2015: The JRA-55 reanalysis: General specifications and basic characteristics. *J. Meteor. Soc. Japan*, **93**, 5–48, https://doi.org/10.2151/jmsj.2015-001.

Kulie, M. S., and R. Bennartz, 2009: Utilizing space-borne radars to retrieve dry snowfall. *J. Appl. Meteor. Climatol.*, **48**, 2564–2580, https://doi.org/10.1175/2009JAMC2193.1.

Kwok, R., S. S. Pang, and S. Kacimi, 2017: Sea ice drift in the Southern Ocean: Regional patterns, variability, and trends. *Elem. Sci. Anthrop*, **5**, 32, https://doi.org/10.1525/elementa.226.

Legates, D. R., 1995: Global and terrestrial precipitation: A comparative assessment of existing climatologies. *Int. J. Climatol.*, **15**, 237–258, https://doi.org/10.1002/joc.3370150302.

Lemonnier, F., and Coauthors, 2019: Evaluation of CloudSat snowfall rate profiles by a comparison with in situ micro-rain radar observations in East Antarctica. *Cryosphere*, **13**, 943–954, https://doi.org/10.5194/tc-13-943-2019.

Leonard, K. C., and R. I. Cullather, 2008: Snowfall measurements in the Amundsen and Bellingshausen Seas, Antarctica. Proc. *65th Eastern Snow Conf.*, Fairlee, VT, 87–98.

——, and T. Maksym, 2011: The importance of wind-blown snow redistribution to snow accumulation on Bellingshausen Sea ice. *Ann. Glaciol.*, **52**, 271–278, https://doi.org/10.3189/172756411795931651.

Lewis, E. L., E. P. Jones, P. Lemke, T. D. Prowse, and P. Wadhams, Eds., 2012: *The Freshwater Budget of the Arctic Ocean.* Springer, 623 pp.

Lindsay, R., M. Wensnahan, A. Schweiger, and J. Zhang, 2014: Evaluation of seven different atmospheric reanalysis products in the Arctic. *J. Climate*, **27**, 2588–2606, https://doi.org/10.1175/JCLI-D-13-00014.1.

Lubin, D., B. Chen, D. H. Bromwich, R. C. Somerville, W. H. Lee, and K. M. Hines, 1998: The impact of Antarctic cloud radiative properties on a GCM climate simulation. *J. Climate*, **11**, 447–462, https://doi.org/10.1175/1520-0442(1998)011<0447:TIOACR>2.0.CO;2.

Maksym, T., and T. Markus, 2008: Antarctic sea ice thickness and snow-to-ice conversion from atmospheric reanalysis and passive microwave snow depth. *J. Geophys. Res.*, **113**, C02S12, https://doi.org/10.1029/2006JC004085.

Markus, T., and Coauthors, 2017: The Ice, Cloud, and Land Elevation Satellite-2 (ICESat-2): Science requirements, concept, and implementation. *Remote Sens. Environ.*, **190**, 260–273, https://doi.org/10.1016/j.rse.2016.12.029.

Marsland, S. J., and J.-O. Wolff, 2001: On the sensitivity of Southern Ocean sea ice to the surface freshwater flux: A model study. *J. Geophys. Res.*, **106**, 2723–2741, https://doi.org/10.1029/2000JC900086.

Martinson, D. G., 1990: Evolution of the Southern Ocean winter mixed layer and sea ice: Open ocean deepwater formation and ventilation. *J. Geophys. Res.*, **95**, 11 641–11 654, https://doi.org/10.1029/JC095iC07p11641.

Maslanik, J., and J. Stroeve, 1990: DMSP SSM/I daily polar gridded brightness temperatures. National Snow and Ice Data Center, CD-ROM.

Massom, R. A., and Coauthors, 2001: Snow on Antarctic sea ice. *Rev. Geophys.*, **39**, 413–445, https://doi.org/10.1029/2000RG000085.

Milani, L., and Coauthors, 2018: CloudSat snowfall estimates over Antarctica and the Southern Ocean: An assessment of independent retrieval methodologies and multi-year snowfall analysis. *Atmos. Res.*, **213**, 121–135, https://doi.org/10.1016/j.atmosres.2018.05.015.

Molod, A., 2012: Constraints on the profiles of total water PDF in AGCMs from AIRS and a high-resolution model. *J. Climate*, **25**, 8341–8352, https://doi.org/10.1175/JCLI-D-11-00412.1.

——, L. Takacs, M. Suarez, and J. Bacmeister, 2015: Development of the GEOS-5 atmospheric general circulation model. Evolution from MERRA to MERRA2. *Geosci. Model Dev.*, **8**, 1339–1356, https://doi.org/10.5194/gmd-8-1339-2015.

Moorthi, S., H. L. Pan, and P. Caplan, 2001: Changes to the 2001 NCEP operational MRF/AVN global analysis/forecast system. NWS Tech. Proc. Bull. 484, 14 pp.

Nicolas, J. P., and D. H. Bromwich, 2011: Precipitation changes in high southern latitudes from global reanalyses: A cautionary tale. *Surv. Geophys.*, **32**, 475–494, https://doi.org/10.1007/s10712-011-9114-6.

Nicolaus, M., and Coauthors, 2017: Snow height and air temperature on sea ice from Snow Buoy measurement, Alfred Wegener Institute, Helmholtz Center for Polar and Marine Research, accessed January 2019, https://doi.org/10.1594/PANGAEA.875638.

Overland, J. E., and Coauthors, 2016: Nonlinear response of mid-latitude weather to changing Arctic. *Nat. Climate Change*, **6**, 992–999, https://doi.org/10.1038/nclimate3121.

Palerme, C., J. E. Kay, C. Genthon, T. S. L'Ecuyer, N. B. Wood, and C. Claud, 2014: How much snow falls on the Antarctic ice sheet. *Cryosphere*, **8**, 1279–1304, https://doi.org/10.5194/tcd-8-1279-2014.

——, C. Claud, A. Dufour, C. Genthon, N. B. Wood, and T. L'Ecuyer, 2017: Evaluation of Antarctic snowfall in global meteorological reanalyses. *Atmos. Res.*, **190**, 104–112, https://doi.org/10.1016/j.atmosres.2017.02.015.

Papritz, L., S. Pfahl, I. Rudeva, I. Simmonds, H. Sodemann, and H. Wernli, 2014: The role of extratropical cyclones and fronts for Southern Ocean freshwater fluxes. *J. Climate*, **27**, 6205–6224, https://doi.org/10.1175/JCLI-D-13-00409.1.

Parish, T. R., 1983: The influence of the Antarctic Peninsula on the wind field over the western Weddell Sea. *J. Geophys. Res.*, **88**, 2684–2692, https://doi.org/10.1029/JC088iC04p02684.

——, and D. H. Bromwich, 2007: Reexamination of the near-surface airflow over the Antarctic continent and implications on atmospheric circulations at high southern latitudes. *Mon. Wea. Rev.*, **135**, 1961–1973, https://doi.org/10.1175/MWR3374.1.

Pauling, A. G., C. M. Bitz, I. J. Smith, and P. J. Langhorne, 2016: The response of the Southern Ocean and Antarctic sea ice to fresh water from ice shelves in an Earth system model. *J. Climate*, **29**, 1655–1672, https://doi.org/10.1175/JCLI-D-15-0501.1.

Perovich, D. K., T. C. Grenfell, B. Light, and P. V. Hobbs, 2002: Seasonal evolution of the albedo of multiyear Arctic sea ice. *J. Geophys. Res.*, **107**, 8044, https://doi.org/10.1029/2000JC000438.

Pope, A., P. Wagner, R. Johnson, J. D. Shutler, J. Baeseman, and L. Newman, 2017: Community review of Southern Ocean satellite data needs. *Antarct. Sci.*, **29**, 97–138, https://doi.org/10.1017/S0954102016000390.

Reynolds, R. W., N. A. Rayner, T. M. Smith, D. C. Stokes, and Q. Wang, 2002: An improved in situ and satellite SST analysis for climate. *J. Climate*, **15**, 1609–1625, https://doi.org/10.1175/1520-0442(2002)015<1609:AIISAS>2.0.CO;2.

——, T. M. Smith, C. Liu, D. B. Chelton, K. S. Casey, and M. G. Schlax, 2007: Daily high-resolution-blended analyses for sea surface temperature. *J. Climate*, **20**, 5473–5496, https://doi.org/10.1175/2007JCLI1824.1.

Rienecker, M. M., and Coauthors, 2011: MERRA: NASA's Modern-Era Retrospective Analysis for Research and Applications. *J. Climate*, **24**, 3624–3648, https://doi.org/10.1175/JCLI-D-11-00015.1.

Saha, S., and Coauthors, 2010: The NCEP Climate Forecast System Reanalysis. *Bull. Amer. Meteor. Soc.*, **91**, 1015–1057, https://doi.org/10.1175/2010BAMS3001.1.

Serreze, M. C., A. P. Barrett, and F. Lo, 2005: Northern high-latitude precipitation as depicted by atmospheric reanalyses and satellite retrievals. *Mon. Wea. Rev.*, **133**, 3407–3430, https://doi.org/10.1175/MWR3047.1.

Sevruk, B., 1982: Methods of correction for systematic error in point precipitation measurement for operational use. WMO Operational Hydrology Rep. 21, 91 pp.

Smith, R. N. B., 1990: A scheme for predicting layer clouds and their water content in a general circulation model. *Quart. J. Roy. Meteor. Soc.*, **116**, 435–460, https://doi.org/10.1002/qj.49711649210.

Sobel, A. H., E. D. Maloney, G. Bellon, and D. M. Frierson, 2008: The role of surface heat fluxes in tropical intraseasonal 26 oscillations. *Nat. Geosci.*, **1**, 653–657, https://doi.org/10.1038/ngeo312.

——, ——, ——, and ——, 2010: Surface fluxes and tropical intraseasonal variability: A reassessment. *J. Adv. Model. Earth Syst.*, **2**, 2, https://doi.org/10.3894/JAMES.2010.2.2.

Sodemann, H., and A. Stohl, 2009: Asymmetries in the moisture origin of Antarctic precipitation. *Geophys. Res. Lett.*, **36**, L22803, https://doi.org/10.1029/2009GL040242.

Sotiropoulou, G., J. Sedlar, R. Forbes, and M. Tjernström, 2015: Summer Arctic clouds in the ECMWF forecast model: An evaluation of cloud parameterization schemes. *Quart. J. Roy. Meteor. Soc.*, **142**, 387–400, https://doi.org/10.1002/qj.2658.

Souverijns, N., and Coauthors, 2018: Evaluation of the CloudSat surface snowfall product over Antarctica using ground-based precipitation radars. *Cryosphere*, **12**, 3775–3789, https://doi.org/10.5194/tc-12-3775-2018.

Stammerjohn, S., and T. Maksym, 2017: Gaining (and losing) Antarctic sea ice: Variability, trends and mechanisms. *Sea Ice,* D. N. Thomas, Ed., Wiley, 261–289, https://doi.org/10.1002/9781118778371.ch10.

Stephens, G. L., and Coauthors, 2008: CloudSat mission: Performance and early science after the first year of operation. *J. Geophys. Res.*, **113**, D00A18, https://doi.org/10.1029/2008JD009982.

Sturm, M., and R. A. Massom, 2017: Snow in the sea ice system: Friend or foe. *Sea Ice*, D. N. Thomas, Ed., Wiley, 65–109, https://doi.org/10.1002/9781118778371.ch10.

——, D. K. Perovich, and J. Holmgren, 2002: Thermal conductivity and heat transfer through the snow on the ice of the Beaufort Sea. *J. Geophys. Res.*, **107**, 8043, https://doi.org/10.1029/2000JC000409.

Sundqvist, H., 1998: Parameterization of condensation and associated clouds in models for weather prediction and general simulation. *Physically-Based Modelling and Simulations of Climate and Climatic Change—Part I*, M. E. Schlesinger, Ed., D. Reidel, 433–461.

Takacs, L. L., M. J. Surez, and R. Todling, 2016: Maintaining atmospheric mass and water balance in reanalyses. *Quart. J. Roy. Meteor. Soc.*, **142**, 1565–1573, https://doi.org/10.1002/qj.2763.

Tanelli, S., S. L. Durden, E. Im, K. S. Pak, D. G. Reinke, P. Partain, J. M. Haynes, and R. T. Marchand, 2008: CloudSat's cloud profiling radar after two years in orbit: Performance, calibration, and processing. *IEEE Trans. Geosci. Remote Sens.*, **46**, 3560–3573, https://doi.org/10.1109/TGRS.2008.2002030.

Tiedtke, M., 1993: Representation of clouds in large-scale models. *Mon. Wea. Rev.*, **121**, 3040–3061, https://doi.org/10.1175/1520-0493(1993)121<3040:ROCILS>2.0.CO;2.

Tietäväinen, H., and T. Vihma, 2008: Atmospheric moisture budget over Antarctica and the Southern Ocean based on the ERA-40 reanalysis. *Int. J. Climatol.*, **28**, 1977–1995, https://doi.org/10.1002/joc.1684.

Tompkins, A., 2002: A prognostic parameterization for the subgrid-scale variability of water vapor and clouds in large-scale models and its use to diagnose cloud cover. *J. Atmos. Sci.*, **59**, 1917–1942, https://doi.org/10.1175/1520-0469(2002)059<1917:APPFTS>2.0.CO;2.

Trenberth, K. E., 2011: Changes in precipitation with climate change. *Climate Res.*, **47**, 123–138, https://doi.org/10.3354/cr00953.

Tromeur, E., and W. B. Rossow, 2010: Interaction of tropical deep convection with the large-scale circulation in the MJO. *J. Climate*, **23**, 1837–1853, https://doi.org/10.1175/2009JCLI3240.1.

Turner, J., and S. Pendlebury, 2004: *The International Antarctic Weather Forecasting Handbook*. British Antarctic Survey, 685 pp.

——, T. A. Lachlan-Cope, J. P. Thomas, and S. R. Colwell, 1995: The synoptic origins of precipitation over the Antarctic Peninsula. *Antarct. Sci.*, **7**, 327–337, https://doi.org/10.1017/S0954102095000447.

Uotila, P., T. Vihma, A. B. Pezza, I. Simmonds, K. Keay, and A. H. Lynch, 2011: Relationships between Antarctic cyclones and surface conditions as derived from high-resolution numerical weather prediction data. *J. Geophys. Res.*, **116**, D07109, https://doi.org/10.1029/2010JD015358.

Warren, S. G., 1982: Optical properties of snow. *Rev. Geophys.*, **20**, 67–89, https://doi.org/10.1029/RG020i001p00067.

Watkins, K., and Coauthors, 2007: Fighting climate change: Human solidarity in a divided world. Human Development Rep., 2007/2008, Palgrave Macmillian for United Nations Development Program, 399 pp.

Webster, M., and Coauthors, 2018: Snow in the changing sea-ice systems. *Nat. Climate Change*, **8**, 946–953, https://doi.org/10.1038/s41558-018-0286-7.

Wingham, D. J., and Coauthors, 2006: CryoSat: A mission to determine the fluctuations in Earth's land and marine ice fields. *Adv. Space Res.*, **37**, 841–871, https://doi.org/10.1016/j.asr.2005.07.027.

Wood, N. B., T. S. L'Ecuyer, D. G. Vane, G. L. Stephens, and P. Partain, 2013: Level 2C Snow-Profile Process Description and Interface Control Document, Algorithm Version P R04. Accessed 3 December 2018, https://www.cloudsat.cira.colostate.edu/sites/default/files/products/files/2C-SNOW-PROFILE_PDICD.P_R04.20130210.pdf.

Worby, A. P., R. A. Massom, I. Allison, V. I. Lytle and P. Heil, 1998: East Antarctic sea ice: A review of its structure, properties and drift. *Antarctic Sea Ice: Physical Processes, Interactions and Variability,* Vol. 74, Antarctic Research Series, Wiley, 41–67, https://doi.org/10.1029/AR074p0041.

Yang, D., and Coauthors, 1995: Accuracy of Tretyakov precipitation gauge: Result of WMO intercomparison. *Hydrol. Processes*, **9**, 877–895, https://doi.org/10.1002/hyp.3360090805.

Zhang, C., 2005: Madden-Julian Oscillation. *Rev. Geophys.*, **43**, RG2003, https://doi.org/10.1029/2004RG000158.